Redox Biology 29 (2020) 101402

Contents lists available at ScienceDirect

Redox Biology

journal homepage: www.elsevier.com/locate/redox

miR-30-5p-mediated ferroptosis of trophoblasts is implicated in the pathogenesis of preeclampsia

Heng Zhang[b,1], Yue He[a,1], Jian-xia Wang[c], Ming-hua Chen[a], Jian-juan Xu[a], Min-hui Jiang[a], Ya-ling Feng[a,*], Yan-fang Gu[a]

[a] Department of Obstetrics and Gynecology, Wuxi Matemal and Child Health Hospital Affiliated to Nanjing Medical University, Wuxi, Jiangsu Province, 214002, PR China
[b] Department of Child Health Care, Wuxi Maternity and Child Health Hospital Affiliated to Nanjing Medical University, Wuxi, Jiangsu Province, 214002, China
[c] Department of Women Health Care, Wuxi Maternity and Child Health Hospital Affiliated to Nanjing Medical University, Wuxi, Jiangsu Province, 214002, China

ARTICLE INFO

Keywords:
miR-30-5p
Ferroptosis
Preeclampsia
SLC7A11
Ferroportin 1

ABSTRACT

Oxidative stress is a major cause of adverse outcomes in preeclampsia (PE). Ferroptosis, i.e. programmed cell death from iron-dependent lipid peroxidation, likely mediates PE pathogenesis. We evaluated specific markers for ferroptosis in normal and PE placental tissues, using *in vitro* (trophoblasts) and in vivo (rat) models. Increase in malondialdehyde content and total Fe^{2+} along with reduced the glutathione content and glutathione peroxidase activity was observed in PE placenta. While the trophoblasts experienced death under hypoxia, inhibitors of ferroptosis, apoptosis, autophagy, and necrosis increased the cell viability. Microarrays, bioinformatic analysis, and luciferase reporter assay revealed that upregulation of miR-30b-5p in PE models plays a pivotal role in ferroptosis, by downregulating Cys2/glutamate antiporter and PAX3 and decreasing ferroportin 1 (an iron exporter) expression, resulting in decreased GSH and increased labile Fe^{2+}. Inhibition of miR-30b-5p expression and supplementation with ferroptosis inhibitors attenuated the PE symptoms in rat models, making miR-30b-5p a potential therapeutic target for PE.

1. Introduction

Preeclampsia (PE) is a pregnancy disease characterized by clinical symptoms such as hypertension and proteinuria, which occur after the 20th gestational week. It affects 7%–10% of pregnancies, and presents high maternal and perinatal mortality [1]. It is widely accepted that PE pathogenesis is associated with the malfunction of extravillous trophoblast (EVT) migration and invasion toward uterine spiral arteries, followed by disordered neovascularization and increased uteroplacental vascular resistance. The abnormal placental development leads to local hypoxia and ischemia, considered the leading cause of overproduction of reactive oxygen species (ROS) [2,3]. Although ROS generation has been associated with multiple organ injuries responsible for the clinical manifestations of PE, the detailed mechanism of impairments caused by ROS is not completely understood.

Ferroptosis is a novel form of programmed cell death that has been found to be associated with oxidative stress. Ferroptosis is quite different from apoptosis, necrosis, and autophagy, in terms of the morphology, biochemistry, and genetics. It is caused mainly by iron-dependent lipid-peroxidative damage. This iron species, primarily referred to as Fe^{2+} [ferrous, Fe(II)], is highly reactive and toxic, as it contributes to the generation of hydroxyl radical, a type of ROS with very strong oxidative characteristics [4]. Normally, iron exists in Fe^{3+} (ferric) state, which is dynamically regulated by the iron transporters in cell membrane or stored in bound form with proteins such as transferrin, ferritin, and NGAL. However, if the regulatory system is impaired under pathological conditions, the increased Fe^{3+} readily undergoes a single electron transfer reaction and converts to Fe^{2+}. GPX4 is a key anti-oxidative enzyme that is capable of preventing the generation of lipid hydroperoxides caused by ROS [5]. However, the protective action of GPX4 requires the participation of glutathione (GSH) as the substrate. Cys2/glutamate antiporter (system Xc^-, SLC7A11) facilitates the acquisition of cystine by cells for the synthesis of GSH. Inhibition of Xc^- decreases the intracellular GSH, thereby leading to the accumulation of lipid hydroperoxides and subsequently, ferroptosis [6,7].

miRNAs belong to small, non-coding RNAs that normally contain 22 nucleotides. One well-recognized function of miRNAs is that they bind to 3' untranslated region of the specific messenger RNAs (mRNA) and further induce a rapid degradation of mRNA. Therefore, miRNAs

* Corresponding author.
E-mail address: 13600182648@163.com (Y.-l. Feng).
[1] Heng Zhang and Yue He were ranked as co-first authors.

https://doi.org/10.1016/j.redox.2019.101402
Received 7 August 2019; Received in revised form 2 December 2019; Accepted 6 December 2019
Available online 09 December 2019

generally function as a negative regulator of specific genes. Recent studies have indicated an important role of microRNAs in the pathophysiology of PE [8–10]. A study reported that miRNA-30a-3p was up-regulated in the placentas of patients with PE, which caused the down-regulation of IGF-1 by miRNA-30a-3p [8]. Down-regulated of IGF-1 was associated to the inhibition of trophoblast invasion [8]. In addition, the levels of some miRNAs were found to be abnormally changed in the placentas or blood of patients with PE. Their abnormal change was used for the evaluation of PE occurrence or severity [9,10], but the mechanism by which these miRNAs affect the occurrence and development of PE were not completely understood.

To our knowledge, ferroptosis has never been reported in PE pathogenesis. The present study for the first time found that many key proteins implicated in the regulation of ferroptosis were aberrantly expressed in the placental tissues of patients with PE, with a notable increase in the lipid oxidation level. Treatment with ferroptosis inhibitors improved the viability of trophoblasts under hypoxic conditions and attenuated the PE symptoms in a rat model. Together, these results suggested that ferroptosis occurs in the placental tissues of patients with PE. We further explored the mechanisms underlying the occurrence of ferroptosis and investigated the damage caused by it. The results would help further elucidate the PE pathogenesis and improve the therapeutic protocols.

2. Materials and methods

2.1. Tissue samples

The study population included patients with PE (n = 18) and physiologically normal pregnancies (n = 18). All of them had undergone cesarean deliveries during Jan. 2017 to Dec. 2017 at the Department of Gynecology and Obstetrics in Wuxi Maternity and Children Health Hospital Affiliated Nanjing Medical University (Wuxi, Jiangsu, China). Patients with cardiovascular diseases, diabetes, metabolic syndrome, infections, kidney disease, congenital malformations, and chromosomal anomalies (number and/or structure) were excluded. The clinical data of the patients is presented in Table 1. Placental tissue samples were randomly collected from the basal plate (2 cm from the periphery, avoiding placental infarcts) immediately after delivery. The tissue samples were stored in formaldehyde or immediately frozen in liquid nitrogen, and then stored at −80 °C until analysis. This study was conducted in accordance with the principles expressed in the Declaration of Helsinki. This study was approved by the Research Medical Ethics Committee of Wuxi Maternity and Children Health Hospital. All the participants were informed of the investigational nature of the study, and written informed consent was obtained from them. The placental biopsies for immunohistochemistry were dixed in 4% paraformaldehyde and embedded in paraffin. The other samples for mRNA analysis were immediately washed to remove blood in a PBS 1X solution, and frozen at −80 °C until analysis.

2.2. Analysis of GSH content and GPX activity

The tissue and cell samples were lysed with 5% 5-sulfosalicylic acid solution. The cellular level of glutathione was determined using a Glutathione Assay Kit (Sigma-Aldrich, St. Louis, MO, USA), following the manufacturer's protocol. GPX activity was analyzed using the Glutathione Peroxidase Assay Kit (ab102530; Abcam), as per the manufacturer's instructions.

2.3. Malondialdehyde (MDA) measurement

The tissue and cell samples were lysed, and the supernatant (2 mL) was mixed with 2 mL of 0.6% thiobarbituric acid in a 10-mL tube. The tube was then heated in boiling water bath for 15 min, followed by thawing on ice, and the optical density of the solution was measured at 532 nm. The results were expressed as μmol MDA/mg protein.

Table 1
Clinical information on patients with PE and healthy controls.

Patient number	Age(years)	Gestational weeks	Urine protein (mg/24 h)	MAP (mmHg)
N1	26	38	_	95.25
N2	24	39 + 3	_	90.41
N3	31	39 + 2	_	89.36
N4	30	38 + 1	_	92.1
N5	34	38	_	88.42
N6	22	37 + 1	_	85.83
N7	25	35 + 6	_	89.31
N8	32	36 + 3	_	90.84
N9	27	38 + 4	_	97.86
N10	26	35 + 5	_	103.87
N11	29	40 + 3	_	105.69
N12	25	39	_	86.62
N13	30	37	_	85.43
N14	27	38 + 3	_	96.17
N15	25	37 + 5	_	105.34
N16	26	34 + 2	_	84.62
N17	28	36	_	92.87
N18	26	35 + 3	_	94.17
P1	33	31 + 4	4090	136.37
P2	30	33 + 3	1135	126.74
P3	34	31	3931	113.05
P4	25	32 + 3	1240	120.67
P5	24	28 + 4	2037	118.2
P6	28	34 + 3	162	121.67
P7	33	37 + 2	1536	134.55
P8	28	33 + 4	1846	138.16
P9	31	30 + 5	2499	131.4
P10	28	35 + 6	2803	117.33
P11	24	34 + 1	1588	135.27
P12	26	37 + 4	2974	122.63
P13	25	36	3058	119.33
P14	27	34 + 3	2018	128.43
P15	27	36 + 2	2493	115.33
P16	23	35 + 2	3349	130.73
P17	23	35	3575	127.17
P18	25	35 + 4	1764	112.67

N: normal controls; P: preeclampsia patients.

2.4. Western blot assay

The tissue and cell samples were lysed with cold radioimmunoprecipitation (RIPA) butter (Bio-Rad, CA, USA). Lysates were heated at 95 °C for 5 min and loaded on 10% gels (Bio-Rad) for SDS–polyacrylamide gel electrophoresis. After electrophoretic separation, the proteins were transferred onto 0.2-μm nitrocellulose membranes (Amersham, Germany), blocked with 5% nonfat milk [in tris-buffered saline (TBS) + 0.01% Tween], and incubated overnight at 4 °C with the primary antibodies targeting: Pax3 (1:500; ab180754, Abcam, Cambridge, UK), POU3F2 (1:500; ab137469), BHLHE40 (1:500; ab23797), GPx4 (1:1000; ab231174; Abcam), SLC7A11/Xc^- (1:500; ab175186, Abcam), FPN1 (1:1000; 26601-1-AP, Proteintech Group, shanghai, China), FTH1 (1:500; ab75972, Abcam), TFR1 (1:1000; 10084-2-AP, Proteintech Group), TFR2 (1:500; sc-32271, Santa Cruz, TX, USA), LC3B (1:500; ab168831, Abcam), and GAPDH (1:3000; ab125247, Abcam). Membranes were washed and incubated with horseradish peroxidase-labeled secondary antibody (Cell Signaling Technology) for 1 h. The antibody-labeled proteins were detected by chemiluminescence using the SuperSignal West Femto Maximum Sensitivity Substrate (Thermo Fisher Scientific, Inc.), in a LAS-3000 Luminescent Image Analyzer (Fujifilm Holdings Corporation, Tokyo, Japan).

2.5. Immunohistochemistry (IHC)

Human placental tissues from uncomplicated or preeclamptic pregnancies were used for IHC assay. Paraffin sections (5 μm) were cut and deparaffinized. Optimal staining was achieved with heat-induced antigen retrieval method, using 10 mmol/L citric acid, pH 6.00. Endogenous peroxidase was quenched with 3% H_2O_2 in ddH_2O for 15 min. To block nonspecific binding, the slides were incubated at 37 °C with 2.5% normal horse serum in PBS for 30 min. This was followed by overnight incubation with antibodies mentioned for the western blot assay (1:500) at 4 °C. The slides were then rinsed in PBS and further incubated with an anti-IgG secondary antibody (1:200; Abcam, Cambridge, MA, USA) at room temperature for 30 min. Each section was immersed in 500 μL of a diaminobenzidine working solution at room temperature for 3–10 min.

2.6. Microarray analyses

The levels of miRNA expression in placenta of patients with PE (n = 3) and physiologically normal pregnancies (n = 3) were analyzed using Human OneArray® v7 Microarrays (OneArray, Shanghai, China). Moreover, the changes of mRNA expression profiles in HTR-8/SVneo cells after down-regulating miR-30b-5p under hypoxia were also analyzed using Human OneArray® v7 Microarrays. Total mRNA was extracted with the RNeasy Kit (Qiagen) to prepare the cyanine 3 (Cy3)-labeled complementary RNA (cRNA). A total of 0.60 μg of Cy3-labeled cRNA was fragmented and hybridized to the Human Microarray for 17 h. The slides were washed and scanned immediately on an Agilent DNA Microarray Scanner (G2565CA) using the one-color scan setting for 8 × 60 K array slides. The scanned images were analyzed in Feature Extraction Software 10.10 (Agilent) with default parameters to obtain background-subtracted and spatially detrended processed signal intensities.

2.7. Reverse-quantitative polymerase chain reaction (RT-qPCR)

Total RNA was extracted from frozen placental tissues and cultured cells using TRI reagent (Sigma-Aldrich), according to the manufacturer's instructions, and 500 ng of the RNA were used for reverse transcription (Thermo Scientific, Whaltham, MA, USA). Real-time PCR was carried out using QuantiNova SYBR Green PCR Kit (Qiagen) and a final concentration of 0.3 nM gene specific primer. Primers for mRNA expression are shown in Table 2. PCR signals were compared among groups after normalization using U6 RNA expression as the internal reference, calculated using the inverse log of ΔΔCT.

2.8. Cell culture and treatment

HTR-8/SVneo and TEV-1 cells were obtained from ATCC (American Type Culture Collection, Manassas, VA) and maintained in RPMI-1640 medium (Life Technologies, Carlsbad, CA, USA) supplemented with 10% foetal bovine serum (Invitrogen, Carlsbad, CA, USA) and antibiotics (100 U/mL penicillin and 100 μg/mL streptomycin). For regular maintenance, the cells were grown in 75-cm^2 plastic flasks at 37 °C in a 5% CO_2 atmosphere, with media changes every 2–3 days. For hypoxia, the cells were cultured in an AW200SG hypoxic workstation (Electrotek, UK) using a continuous flow of a humidified mixture of 1% O_2, 5% CO_2, and 94% N_2 at 37 °C. Experiments were performed with the cells under either hypoxic (2% O2) or normoxic (20% O_2, as a control) conditions.

Inhibitors of apoptosis (20 μM Z-DEVD-FMK, Apexbio, Shanghai, China), autophagy (0.5 mM 3-Methyladenine, Apexbio), necrosis (0.5 μM Necrostatin-1, Medchemexpress, Shanghai, China), and ferroptosis [60 nM Ferrostatin-1 and 100 μM Deferoxamine mesylate (DFOM), Medchemexpress] were added to cells cultured under hypoxia to determine the mode of cell death caused by hypoxia.

2.9. Measurements of total and labile Fe(II) contents

This study measured the total Fe(II), including the free Fe(II) and Fe (II) bound to proteins, in placental tissues. The total Fe(II) levels were determined using an Iron Colorimetric Assay Kit purchased from ScienCell (Cat: 8448). According to the manufacturer's instructions, tissues were added to an iron assay buffer, homogenized on ice, and centrifuged at 13,000 × *g* for 10 min at 4 °C, to obtain the supernatant for the assay. A 50-μL sample was incubated with 50 μL of assay buffer in a 96-well microplate for 30 min at 25 °C. The sample was then incubated with 200 μL of reagent mix in the dark for 30 min at 25 °C, and the absorbance was measured at 593 nm with a microplate reader.

Labile iron (which is primarily in ferrous form) is a small transitional pool of intracellular iron, commonly termed as labile iron pool (LIP). This iron species is loosely bound to endogenous chelators (protein) such as citrate, acetate, malate, phosphate, and adenine nucleotides, making it capable of reacting with oxygen and generating ROS through Fenton chemistry. The LIP levels were measured using calcein-acetoxymethyl ester (calcein-AM, MedChemExpress, NJ, USA) and deferiprone (MedChemExpress), according to the methods described in the literature [11]. Calcein-AM is a nonfluorescent, membrane-permeant dye readily taken up by live cells. Once within the cytoplasm, calcein-AM is cleaved by cytoplasmic esterases releasing the membrane-impermeant calcein fluorophor. Calcein fluorescence is stable, insensitive to pH, but can be quenched rapidly and stoichiometrically by divalent metals such as Fe^{2+} and Co^{2+}, but not by Cd^{2+}

Table 2
The primer sequences for PCR.

Gene name	Primer orientation	Sequences
Pax-3	Forward	5′-CTGGAACATTTGCCCAGACT-3′
	Reverse	5′-TATCCAGGTGAAGGCGAAAC-3′
SLC7A11	Forward	5′-TCTCCAAAGGAGGTTACCTGC-3′
	Reverse	5′-AGACTCCCCTCAGTAAAGTGAC-3′
hsa-miR-489-3p	Forward	5′-ACACTCCAGCTGGGGTGACATCACATATAC-3′
	Reverse	5′-CTCAACTGGTGTCGTGGAGTCGGCAATTCAGTTGAGGCTGCCGT-3′
hsa-miR-30b-5p	Forward	5′-ACACTCCAGCTGGGTGTAAACATCCTACAC-3′
	Reverse	5′-CTCAACTGGTGTCGTGGAGTCGGCAATTCAGTTGAGAGCTGAGT-3′
hsa-miR-30a-3p	Forward	5′-ACACTCCAGCTGGGCTTTCAGTCGGATGTT-3′
	Reverse	5′-CTCAACTGGTGTCGTGGAGTCGGCAATTCAGTTGAGGCTGCAAA-3′
hsa-miR-181a-5p	Forward	5′-ACACTCCAGCTGGGAACATTCAACGCTGTCG-3′
	Reverse	5′-CTCAACTGGTGTCGTGGAGTCGGCAATTCAGTTGAGACTCACCG-3′
Rno-miR-30b-5p	Forward	5′-ACACTCCAGCTGGGTGTAAACATCCTACAC-3′
	Reverse	5′-CTCAACTGGTGTCGTGGAGTCGGCAATTCAGTTGAGAGCTGAGT-3′
U6snRNA	Forward	5′-CTCGCTTCGGCAGCACA-3′
	Reverse	5′-AACGCTTCACGAATTTGCGT-3′

and Mg^{2+}. Deferiprone is high-affinity iron-chelator. Adding deferiprone to calcein-loaded cells can restore the calcein fluorescence. The increase in fluorescence intensity reflected the levels of calcein-bound iron that reflects the amount of LIP. In brief, exponentially growing HTR-8/SVneo and TEV-1 cells were seeded in a 96-well plate at a density of 1×10^4 cells/well. Cells were incubated with 0.5 μM calcein-AM for 15 min at 37 °C. The cells were then washed twice and incubated for 1 h with or without 100 μM deferiprone. Following washing with PBS, the cells were analyzed by a microplate reader with a 488-nm argon- and a 635-nm red diode laser for excitation.

2.10. Cell viability assay

Cell viability was evaluated using the Cell Counting Kit-8 (CCK-8) (LJ621, Dojindo, Japan), according to the manufacturer's instructions. Cells were seeded in 96-well flat bottom microtiter plates at a density of 5,000 cells per well. Twenty-four hours later, the CCK-8 agent was added at the indicated concentrations for 6 h. The absorbance was measured on a microplate reader (Synergy HT, Bio-Tek, United States) at 450 nm.

2.11. Apoptosis assay

Apoptosis was evaluated using Annexin V-PE/7-AAD Apoptosis Kit (KA3809, Abnova, Shanghai, China). Cells were harvested and re-suspended in ice-cold 1× binding buffer at a concentration of 1×10^6 cells/mL. A 100-μL sample of the cell suspension was mixed with 5 μL Annexin V-PE and 5 μL 7-AAD. The mixture was incubated for 15 min at room temperature in the dark and then analyzed by FACS Calibur Flow Cytometer (Beckman Coulter, CytoFLEX S, United States).

2.12. Lactate dehydrogenase (LDH) release assay

Necrosis was analyzed by measuring the activity of LDH released into cell culture supernatants using a LDH assay kit (Beyotime Institute of Biotechnology, Najing, China), according to the manufacturer's protocol.

2.13. Immunofluorescence (IF) assay

Cells were fixed with 4% paraformaldehyde in PBS for 30 min at 4 °C and then blocked with 2% bovine serum albumin (BSA) in PBS. Incubation with the anti-LC3B antibody (1:200, abcam) was carried out for 1 h at 20 °C. This was followed by incubation with secondary anti-IgG antibody conjugated to Alexa Fluor 488 (1:200; ThermoFisher Scientific) for 1 h at 20 °C. Cells were visualized at 400X on an inverted Zeiss Observer microscope (Carl Zeiss, Göttingen, Germany).

2.14. Intracellular ROS measurement

Intracellular ROS was evaluated by using 2,7′-dichlorodihydrofluorescein diacetate (H2DCFDA, Invitrogen). After the above indicated treatments, cells were stained with the H2DCFDA for 10 min, and then washed twice with PBS. Fluorescence of cells in PBS was measured using the FACS Calibur Flow Cytometer.

2.15. Transfection

HTR-8/SVneo and TEV-1 cells (10^5 cells/well) were cultured in 6-well plates. miR-30b-5p mimics and inhibitor, siRNA targeting Pax3, Pax3-and SLC7A11-expressing plasmids and corresponding control vectors, constructed by the GenePharma company (Shanghai, China), were transfected into HTR-8/SVneo and TEV-1 cells using Lipofectamine 2000 (Invitrogen–Life Technologies), following standard protocols. At 36 h post transfection, cells were harvested for further experiments.

2.16. Luciferase reporter assay

Luciferase reporter assay was performed to identify the putative binding sites (seed sequences) for hsa-miR-30b-5p in the 3′-UTR of *pax3* and *SLC7A1*1 mRNA, as predicted by bioinformatic analysis webs, including TargetScan, miRanda, and PicTar. The wild-type (WT) pax3 and SLC7A11 3′-UTR as well as their mutant versions (MT), wherein the putative binding sites were mutated, were synthesized and inserted into a pmirGLO vector (at XhoI and NotI restriction sites; Promega, Madison, WI, USA). The newly synthesized pmirGLO vectors were verified by DNA sequencing. HTR-8/SVneo cells (10^4 cells/well) were seeded in 12-well plates and transfected with WT or MT constructs, together with either hsa-miR-10b-3p mimics or negative control using Lipofectamine 2000 (Invitrogen). Cells were harvested at 48 h and the activity of firefly luciferase was measured and normalized to that of *Renilla* luciferase.

2.17. Chromatin immunoprecipitation (ChIP) assay

The EZ-Magna ChIP kit (EMD Millipore) was used to conduct the ChIP assays in accordance with the manufacturer's protocol. After carrying out the above-mentioned cell treatments, the HTR-8/SVneo cells were lysed with Cell Lysis Buffer and Nuclear Lysis Buffer and sonicated to obtain chromatin fragments. Next, the lysates were immunoprecipitated with Magnetic Protein A Beads conjugated with Pa×3 (Millipore) or IgG (Millipore) as a control. PCR assay was performed to detect the enrichment of *SLC7A11*, *FPN1* and *TFR1* DNA in the precipitated proteins.

2.18. Invasion assay

Invasion assays were performed using transwell plates containing polycarbonate filters with a pore size of 8.0 μm. The transwell inserts were first coated with 50 μL of 1 mg/mL Matrigel matrix (Becton Dickinson, Franklin Lakes, NJ, USA) at 37 °C for 4 h to allow gelling, according to the manufacturer's recommendations. HTR8/SVneo cells were seeded at a density of 1.5×10^5 cells in 200 μL of medium without fetal bovine serum in the upper chamber. The inserts were removed and washed in phosphate-buffered saline (PBS), and the non-migrating cells in the upper chamber were removed with a cotton bud. The inserts were then fixed in cold methanol for 10 min at room temperature and stained with hematoxylin. Cells that invaded the lower surface were counted in 10 fields at 200× magnification.

2.19. Animal study

All animal experiments were approved by the Stanford University Animal Care and Use Committee (Stanford, CA, USA), and conducted according to the National Institutes of Health guidelines for animal welfare. Pregnant SD rats were randomly dived into four groups: sham group (n = 8), PE group (n = 8), PE + ferrostatin-1 group (n = 8), and PE + miR-30b-5p inhibition group (n = 8). On day 14 of pregnancy, PE rat model was established through reduced uterine perfusion pressure (RUPP) surgery, wherein constrictive silver clips were placed on the aorta (0.203-mm clips) superior to the iliac bifurcation and on the ovarian vessels (0.100-mm clips), according to a previous description [12]. Sham rats were operated on in a fashion similar to that of RUPP rats, but without clipping. Mini-pumps were also intraperitoneally inserted into rats on day 14 of pregnancy. The mini-pump in each rat delivered the ferrostatin-1 at a dose of 10 μmol/kg/day for 5 days. An miR-30b-5p antagonist (GenePharma) was injected from the tail veins on day 13 of gestation, at a rate of 100 μL/day for 6 days. The blood pressure was measured on days 14, 16, and 19 of gestation using catheters inserted into the carotid artery and jugular vein.

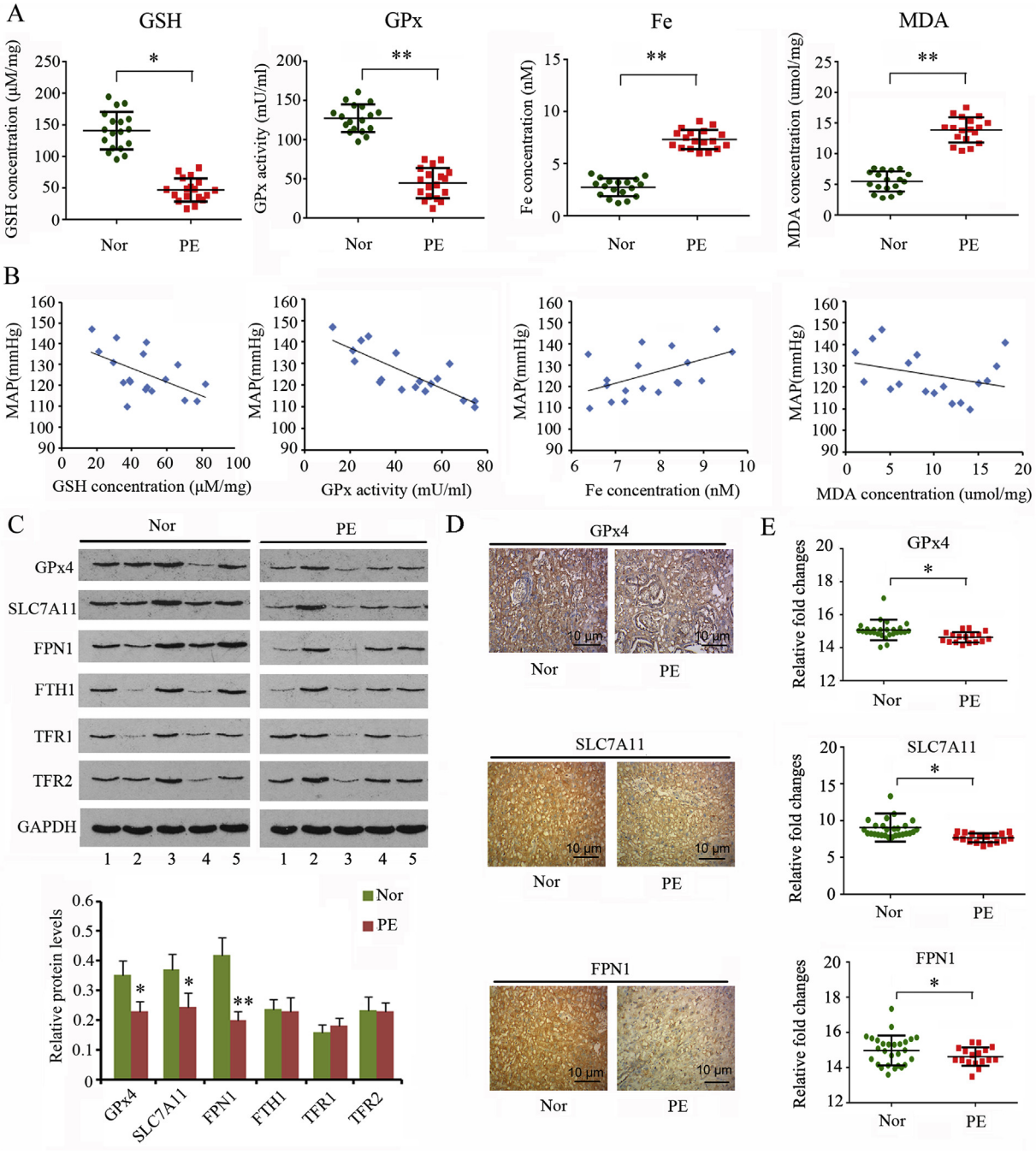

Fig. 1. Evaluation of ferroptosis in the placenta of patients with PE.
Placental tissues were collected from patients with PE (n = 25) as well as from physiologically normal pregnancies (n = 25). (A) GSH content, GPx activity, total Fe (II), and MDA levels were measured using the corresponding detection kits, and (B) their correlations with maternal blood pressure were evaluated using Person correlation coefficient. Levels of proteins closely associated with ferroptosis were assessed using western blot (C) and IHC assays (D). (E) GSE10588 data set demonstrated reduced expression of GPx4, SLC7A11 and FPN1 in PE placental tissues compared to those in physiologically normal pregnancies. Nor: Normal group; PE: Preeclampsia group; *$p < 0.05$, **$p < 0.01$, compared with the normal group.

2.20. Statistics

Data were analyzed using the SPSS 12.0 software (SPSS, Inc., Chicago, IL, USA). Statistical significance of the differences was evaluated using one-way analysis of variance (one-way ANOVA), followed by Scheffe's post-hoc test. P < 0.05 was considered to represent a statistically significant difference.

3. Results

3.1. Ferroptosis likely occurs in the placenta of patients with PE

Ferroptosis is characterized by excessive lipid peroxidation mediated by Fe(II). Our results revealed that both GSH content ($p < 0.05$) and GPx activity ($p < 0.01$) were reduced in the placental tissues of patients with PE compared to those in healthy controls (Fig. 1A). In accordance to their reduction, MDA content conversely increased in the placental tissues of patients with PE ($p < 0.01$). Furthermore,

placental tissues of patients with PE showed a higher concentration of total Fe(II) than healthy controls ($p < 0.01$). Given that blood pressure is one of the most important indices to evaluate the severity of PE, we analyzed the correlation of blood pressure with GSH content, GPx activity, MDA content, and total Fe(II) concentrations. Pearson correlation analysis showed that the blood pressure of the patients with PE was positively correlated with GSH content ($r = 0.549, p < 0.05$) and GPx activity ($r = 0.623, p < 0.05$), but negatively correlated with total Fe (II) concentration ($r = -0.442, p < 0.05$; Fig. 1B). The correlation between the blood pressure and MDA content ($r = -0.314$) was weak.

We further tested the levels of proteins that are associated with ferroptosis. Western blot analysis revealed that GPx4 ($p < 0.05$), SLC7A11 ($p < 0.05$), and FPN1 ($p < 0.01$) protein levels decreased in the placental tissues of patients with PE, whereas the levels of FTH1, TFR1, and TFR2 proteins were not changed (Fig. 1C). Immunohistochemistry also identified the downregulation of Pax3, GPx4, SLC7A11 and FPN1 in PE placental tissues (Fig. 1D). Moreover, we analyzed the data in GO:GSE10588 data set that documented the results of gene expression in placental tissues from PE patients and physiologically normal pregnancies. In accordance to our data, GSE10588 data set demonstrated that GPx4, SLC7A11 and FPN1 were down-regulated in PE placental tissues ($p < 0.05$, Fig. 1E).

3.2. Downregulated Pax3 probably underlies reduced expression of FPN1 in PE placental tissues

Both GSE50783 and GSE44667 data sets provided the data of genes that were aberrantly expressed in placental tissues from PE patients and physiologically normal pregnancies. Transcript factors implicated in the transcription of FPN1 were predicted using a Bioinformatics analysis website (http://bioinfo.life.hust.edu.cn/hTFtarget#!/). To find the reason that caused the reduced expression of FPN1 in PE placental tissues, we initially analyzed the intersection between the aberrantly expressed genes and transcript factors targeting FPN1. As indicated by the Venn diagram, three of the transcript factors (Pax3, POU3F2 and BHLHE40) were found to be aberrantly expressed in placental tissues from PE patients (Fig. 2A). Bioinformatics analysis website Jasper (http://jaspar2016.genereg.net/) gave the highest score on POU3F2 followed by Pax3 (Fig. 2B). A higher score suggests a higher possibility that FPN1 is regulated by the transcript factor. We performed western blot to test the protein levels of these three transcript factors in placental tissues from PE patients and physiologically normal pregnancies. Although mRNA level of POU3F2 was down-regulated in PE placental tissues according to data from GSE50783 and GSE44667 data sets, POU3F2 protein level was not significantly changed (Fig. 2C). Pax3 protein level was down-regulated in PE placental tissues ($p < 0.01$), while BHLHE40 protein level was significantly up-regulated ($p < 0.01$). Results from immunohistochemistry assay (Fig. 2D) and GSE10588 data set ($p < 0.05$, Fig. 2E) also confirmed the down-regulation of Pax3 in PE placental tissues. Based on these data, down-regulated Pax3 is probably a primary cause of FPN1 protein reduction in PE placental tissues. Another transcript factor-predicting websit, Jasper (http://jaspar2016.genereg.net/), showed the motif, a sequence in gene promoter that is recognized by Pax3 (Fig. 2F). Moreover, Jasper revealed two potential binding sites of transcription factor Pax3 at the promoter of *FPN1* and *SLC7A11* genes. Our following study was performed to identify the regulatory effect of Pax3 on *FPN1* and *SLC7A11* expression.

3.3. Higher levels of miR-30b-5p in the placental tissues of patients with PE are likely associated with the downregulation of SLC7A11 and Pax3

miRNAs play an important role in regulating the gene expression at post-transcription level. We performed microarray analysis to identify the miRNAs that were differentially expressed in PE placental tissues. The results showed that 273 miRNAs were upregulated, whereas 235 miRNAs were downregulated, in the PE tissues (Fig. 3A). Bioinformatic analysis using TargetScan, miRmap, and miRanda predicted 607 miRNAs and 1421 miRNAs that target Pax 3 and SLC7A11, respectively. Next, we analyzed the intersection among the upregulated miRNAs and those miRNAs targeting Pax 3 and SLC7A11. As indicated by the Venn diagram, five upregulated miRNAs in PE placental tissues targeted both Pax 3 and SLC7A11 (Fig. 3B). We further performed PCR to identify the expression of these five miRNAs in normal and PE placental tissues. miRNA-30b-5p ($p < 0.01$) and miRNA-489-3p ($p < 0.05$, Fig. 3C) were indeed upregulated in PE placental tissues, with a more profound increase observed for miRNA-30b-5p. In addition to the placental tissues, miRNA-30b-5p was also found to be upregulated in the serum of patients with PE ($p < 0.01$, Fig. 3D). miRNA-30b-5p was the choice for further study of its regulatory effects on SLC7A11 and Pax3.

3.4. Hypoxia causes the ferroptosis of trophoblasts along with apoptosis, autophagy, and necrosis

Hypoxia resulted from disordered neovasucularization in the PE placenta is closely associated with the generation of oxidative stress, therefore the *in vitro* PE model was established by culturing HTR-8/SVneo and TEV-1 cells under hypoxic conditions. The viability of HTR-8/SVneo and TEV-1 cells was decreased in hypoxic conditions compared with normal oxygen conditions ($p < 0.01$, Fig. 4A). To determine the reason for cell death under hypoxia, we added inhibitors of apoptosis, autophagy, necrosis, or ferroptosis to the cells before exposure to hypoxia. All these inhibitors increased the cell viability under hypoxia, with the most pronounced improvement observed for ferroptosis inhibitors ($p < 0.05$).

Next, we analyzed the effect of hypoxia on apoptosis, autophagy, necrosis, and ferroptosis separately. Flow cytometry showed that the apoptosis rate of HTR-8/SVneo and TEV-1 cells was increased by hypoxia ($p < 0.05$, Fig. 4B), but apoptosis inhibitor blocked the increase in the apoptosis rate ($p < 0.05$). Necrosis is associated with cell membrane rupture, resulting in the release of LDH to extracellular space. Therefore, extracellular concentration of LDH is commonly used to evaluate the percentage of cells that undergo necrosis. Hypoxia caused an increase in LDH concentration in the cell culture medium ($p < 0.05$, Fig. 4C). Pretreatment with necrosis inhibitor hindered the increase in LDH concentration by hypoxia ($p < 0.05$). LC3B protein is a biomarker of autophagy. The LC3B protein level was found to be increased in trophoblasts under hypoxia compared with normal oxygen conditions ($p < 0.01$, Fig. 4E). However, the increase in LC3B protein level was inhibited by the autophagy inhibitor ($p < 0.05$). IF assay also confirmed that the autophagy inhibitor blocked the LC3B increase in trophoblasts under hypoxia (Fig. 4D).

In the context of ferroptosis, hypoxia caused a reduction in GSH content ($p < 0.01$, Fig. 5A) and GPx activity in trophoblasts ($p < 0.05$), as well as an increase in labile Fe(II) concentration ($p < 0.05$) and MDA content ($p < 0.01$). One of the ferroptosis inhibitors, ferrostatin-1, reversed the changes in GSH content ($p < 0.01$), GPx activity ($p < 0.05$), and MDA content ($p < 0.05$), but had no effect on labile Fe(II) concentration. Another ferroptosis inhibitor, DFOM reversed the changes in GSH content ($p < 0.05$), labile Fe(II) concentration ($p < 0.05$), and MDA content ($p < 0.05$), but had no effect on GPx activity. ROS levels were increased in both HTR-8/SVneo and TEV-1 cells under hypoxia ($p < 0.01$ or $p < 0.001$, Fig. 5B), however ferrostatin-1 and DFOM blocked the increase of ROS ($p < 0.05$). Western blot analysis showed that hypoxia caused the downregulation of Pax 3 ($p < 0.01$), GPx4 ($p < 0.05$), SLC7A11 ($p < 0.01$), and FPN1 ($p < 0.01$) in both HTR-8/SVneo and TEV-1 cells (Fig. 5C). Except DFOM, which increased the GPx4 expression solely in TEV-1 cells ($p < 0.05$), neither ferrostatin-1 nor DFOM had an effect on the expression of Pax 3, SLC7A11, and FPN1 in HTR-8/SVneo and TEV-1 cells under hypoxia.

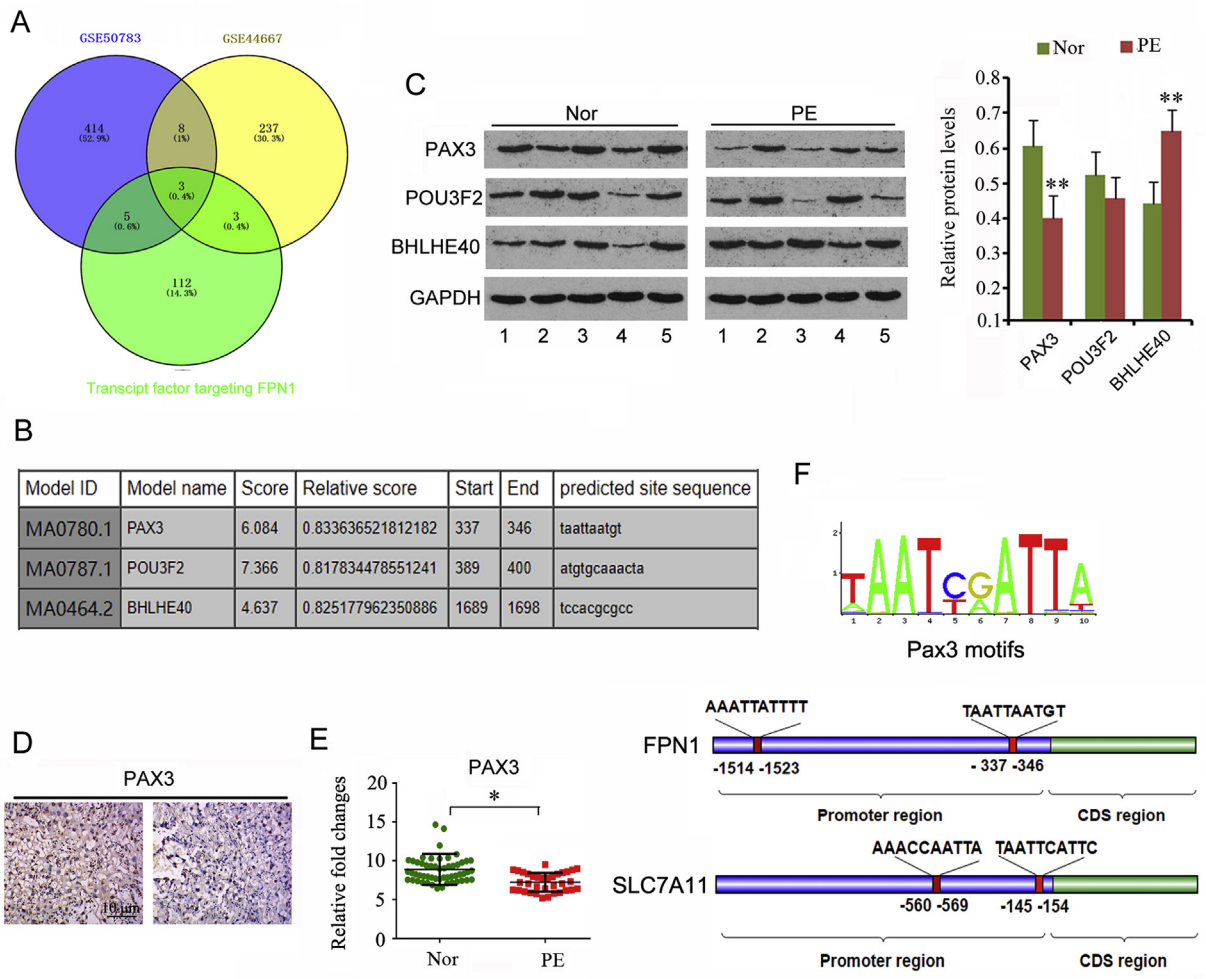

Fig. 2. Downregulated Pax3 probably resulted in reduced expression of FPN1 in PE placental tissues.
Both GSE50783 and GSE44667 data sets provided the data of genes that were aberrantly expressed in placental tissues from PE patients and physiologically normal pregnancies. Transcript factors that were implicated in the transcription of FPN1 were predicted using a Bioinformatics analysis website (http://bioinfo.life.hust.edu.cn/hTFtarget#!/). We analyzed the intersection between the aberrantly expressed genes and transcript factors targeting FPN1. As indicated by the Venn diagram, three of the transcript factors (Pax3, POU3F2 and BHLHE40) were found to be aberrantly expressed in placental tissues from PE patients (A). Bioinformatics analysis website Jasper (http://jaspar2016.genereg.net/) gave the highest score on POU3F2 followed by Pax3 (B). We performed western blot to test the protein levels of these three transcript factors in placental tissues from PE patients and physiologically normal pregnancies (C). Pax3 protein level was down-regulated in PE placental tissues, while BHLHE40 protein level was significantly up-regulated. Results from immunohistochemistry assay (D) and GSE10588 data set (E) also confirmed the down-regulation of PAX3 in PE placental tissues. Another transcript factor-predicting websit, Jasper (http://jaspar2016.genereg.net/), showed the motif, a sequence in gene promoter that is recognized by Pax3 (F). Moreover, Jasper revealed two potential binding sites of transcription factor Pax3 at the promoter of *FPN1* and *SLC7A11* genes. Our following study was performed to identify the regulatory effect of Pax3 on *FPN1* and *SLC7A11* expression. *$p < 0.05$, **$p < 0.01$, compared with the normal group.

3.5. The regulatory effects of miR-30b-5p and Pax3 on gene expression

To confirm the regulatory effect of miR-30b-5p on Pax3 and SLC7A11, we upregulated and downregulated the miR-30b-5p expression using the mimics and inhibitors, respectively. Upregulation of miR-30b-5p was accompanied with a reduction in Pax3 and SLC7A11 expression ($p < 0.05$, Fig. 6A). Conversely, miR-30b-5p depletion resulted in increased Pax3 and SLC7A11 expression ($p < 0.05$). Luciferase reporter assay showed that increasing the miR-30b-5p expression decreased the luciferase activity of Pax3 wild type construct ($p < 0.01$, Fig. 6B), but mutation at both binding sites in the wide type construct partly restored the activity ($p < 0.05$ vs. WT construct). Likewise, increasing the miR-30b-5p expression decreased the luciferase activity of SLC7A11 wide type construct ($p < 0.01$, Fig. 6C), but mutation at the potential binding site in the wild type construct partly restored the activity ($p < 0.05$ vs. WT construct).

As indicated by ChIP assay, Pax3 could bind to the promoters of *SLC7A11*, *FPN1* genes, but not *TFR1* promoter (Fig. 6D). To determine whether Pax3 is involved in the regulation of SLC7A11, FPN1 and TFR1, we knocked Pax3 down in HTR-8/SVneo and TEV-1 cells. Transfection with siRNA-Pax3 decreased the Pax3 protein level ($p < 0.01$), which was associated with a decreased level of FPN1 protein (Fig. 6E). However, the protein levels of SLC7A11 and TFR1 were not changed following Pax3 knockdown.

3.6. The effects of miR-30b-5p, Pax3, and SLC7A11 on the viability, invasion, and ferroptosis of HTR-8/SVneo and TEV-1 cells

As hypoxic treatment increased miR-30b-5p and decreased the Pax3 and SLC7A11 levels in HTR-8/SVneo and TEV-1 cells, we restored their expression to determine whether they are involved in the regulation of viability, invasion, and ferroptosis of HTR-8/SVneo and TEV-1 cells. Transfection with miR-30b-5p inhibitor abolished the increase in the expression of HTR-8/SVneo and TEV-1 cells caused by hypoxic

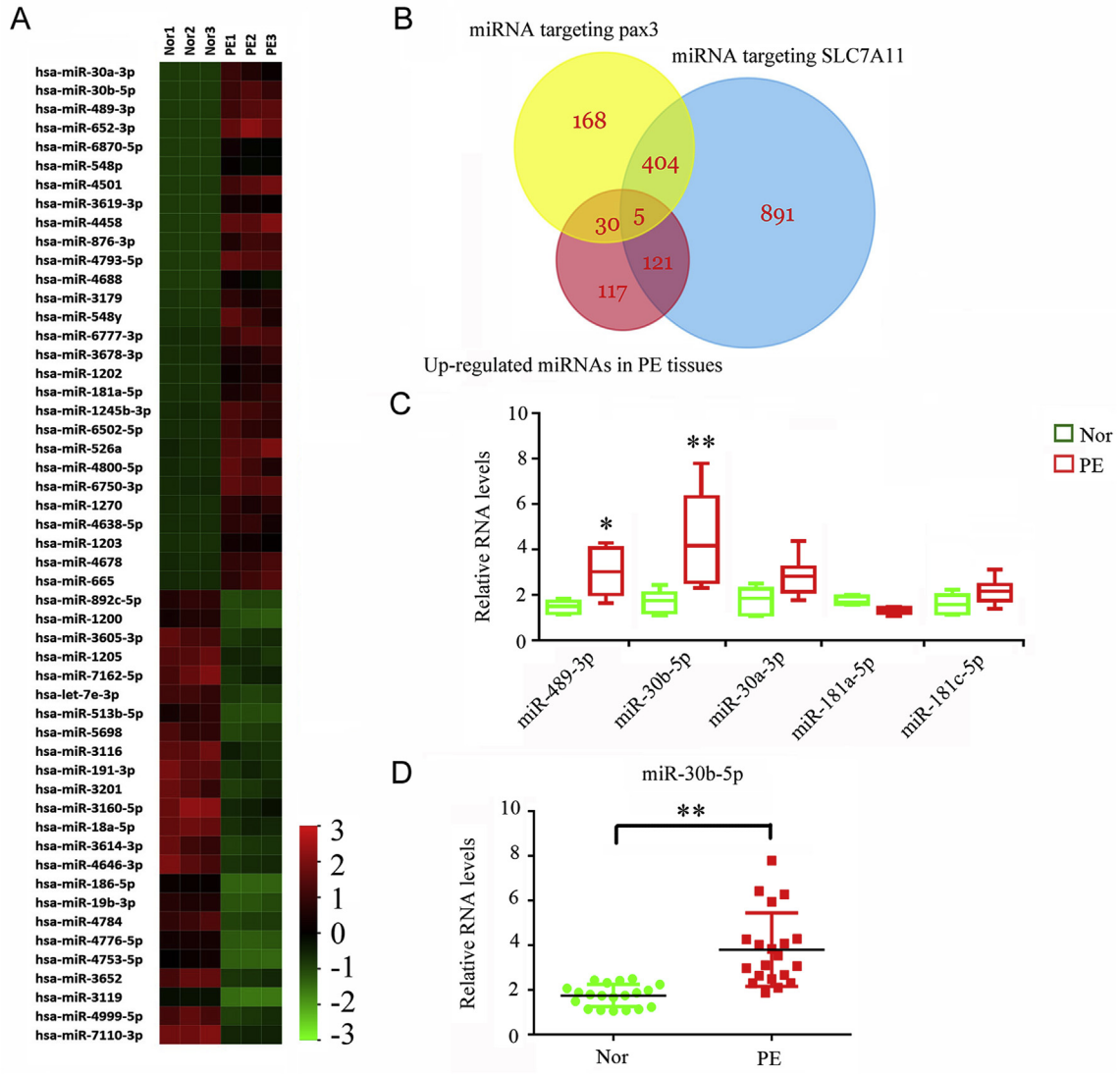

Fig. 3. Identification of miRNAs that likely regulates the expression of SLC7A11 and Pax3.
(A) Microarray detection was performed to find the differentially expressed miRNAs between PE and normal placental tissues. (B) Bioinformatic analysis using TargetScan, miRmap, and miRanda predicted 607 miRNAs and 1421 miRNAs that target Pax 3 and SLC7A11, respectively. Venn diagram showed the intersection among the upregulated miRNAs and those targeting Pax 3 and SLC7A11. PCR was used to quantify the expression of five miRNAs shown in the intersection region of Venn diagram in normal and PE placental tissues (C) as well as miRNA-30b
-5p expression in the normal and PE serum (D).

treatment ($p < 0.01$, Fig. 7A). In addition, preventing the increase of miR-30b-5p under hypoxia almost restored the Pax3, SLC7A11, and FPN1 expression ($p < 0.01$ vs. hypoxia group, Fig. 7A and B). Overexpression of Pax3 and SLC7A11 also abated the reduction in their expression under hypoxia.

Blocking the increase of miR-30b-5p under hypoxia inhibited the reduction in cell viability ($p < 0.05$ vs. hypoxia group, Fig. 7C), invasion capacity ($p < 0.05$ vs. hypoxia group, Fig. 7D), GSH concentration ($p < 0.05$ vs. hypoxia group, Fig. 7E), and GPx activity ($p < 0.05$ vs. hypoxia group), as well as the increase in liable Fe(II) ($p < 0.05$ vs. hypoxia group), MDA concentrations ($p < 0.05$ vs. hypoxia group) and intracellular ROS levels ($p < 0.05$ or $p < 0.01$ vs. hypoxia group, Fig. 7F). Overexpression of Pax3 and SLC7A11 also improved the cell viability, cell invasion, and GSH concentration, and disrupted the increase in MDA and ROS under hypoxia ($p < 0.05$ vs. hypoxia group), although Pax3 overexpression had no positive effect on GPx activity, and SLC7A11 overexpression failed to hinder the increase in liable Fe(II) concentration.

To comprehensively understand the biological processes influenced by miR-30b-5p, we performed Microarray analyses that detected the changes of mRNA expression profiles in HTR-8/SVneo cells after down-regulating miR-30b-5p under hypoxia. Microarray analyses also manifested the up-regulation of Pax3, FPN1 and SLC7A11 after decreasing miR-30b-5p under hypoxia (Fig. 8A and B). We performed GSEA (gene set enrichment analysis) of genes, whose expression was changed with miR-30b-5p knockdown, to reveal the biological processes regulated by miR-30b-5p. Results showed that miR-30b-5p notably influenced various biological processes including cellular response to oxidative stress, regulation of apoptotic process, protein stabilization, signaling pathways mediated by NF-κB, PI3K and PKB, cell differentiation as well as DNA-templated transcription (Fig. 8C).

3.7. Therapeutic effects of miR-30b-5p and ferroptosis inhibitors in PE rat model

PCR analysis showed a higher miR-30b-5p expression in the placenta of PE rats than in the placenta of sham rats ($p < 0.01$, Fig. 9A). The injection of miR-30b-5p antagonist not only prevented the increase

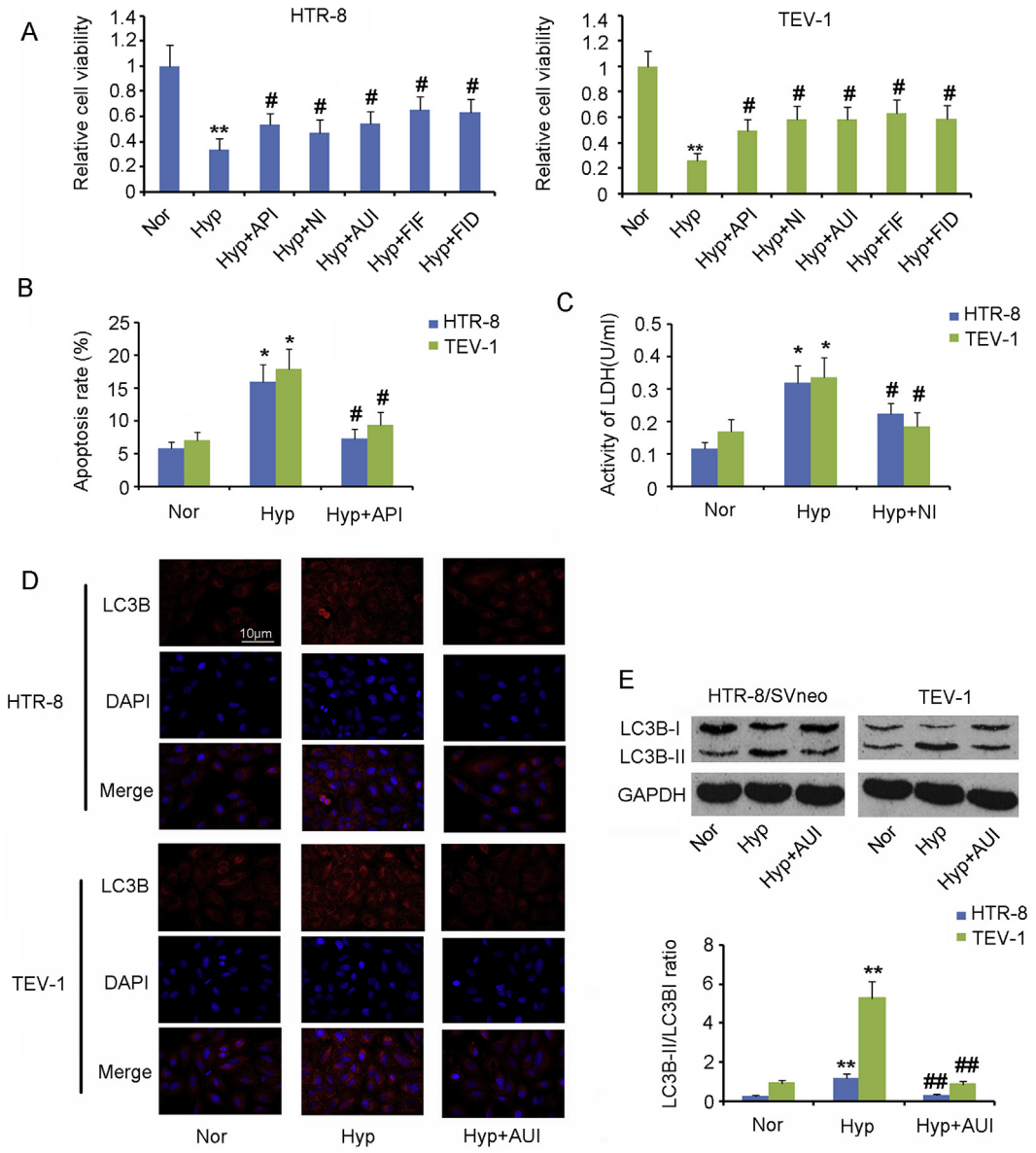

Fig. 4. Hypoxia caused apoptosis, autophagy necrosis, and ferroptosis in trophoblasts.
The *in vitro* PE model was established by culturing HTR-8/SVneo and TEV-1 cells under hypoxic conditions. (A) Inhibitors of apoptosis (20 μM Z-DEVD-FMK), autophagy (0.5 mM 3-Methyladenine), necrosis (0.5 μM Necrostatin-1) and ferroptosis (60 nM Ferrostatin-1 and 100 μM Deferoxamine mesylate) were added to the cells cultured under hypoxia. Twenty-four hours later, the CCK-8 agent was added to determine the cell viability. (B) Flow cytometer was used to assess the apoptosis rate of HTR-8/SVneo and TEV-1 cells. (C) Extracellular concentration of LDH was used to evaluate the percentage of cells that undergo necrosis. LC3B protein levels in cells were assessed using IF (D) and western blot assays (E). Nor: normoxia; Hyp: hypoxia; API: apoptosis inhibitor; NI: necrosis inhibitor; AUI: autophagy inhibitor; FIF: ferroptosis inhibitor, ferrostatin-1; FID: ferroptosis inhibitor Deferoxamine mesylate. $^{*}p < 0.05$, $^{**}p < 0.01$, compared with the HTR-8/SVneo or TEV-1 cells under normoxia; $^{\#}p < 0.05$, $^{\#\#}p < 0.01$, compared with the HTR-8/SVneo or TEV-1 cells under hypoxia.

in miR-30b-5p ($p < 0.01$ vs. PE group), but also abated the reduction in Pax3 ($p < 0.01$ vs. PE group, Fig. 9B), SLC7A11 ($p < 0.01$ vs. PE group), and FPN1 ($p < 0.05$ vs. PE group) in the PE rats. We further determined whether the inhibition of miR-30b-5p expression and ferroptosis conferred any therapeutic effects in the PE rats. Both SDP and DBP showed a gradual increase once the PE model was established ($p < 0.05$ on day 12 and $p < 0.01$ on day 19, Fig. 9C). In addition, the PE rats showed increased urinary protein levels ($p < 0.01$, Fig. 9D) and decreased fetal survival rate ($p < 0.01$, Fig. 9E). Treatments with miR-30b-5p inhibitor and ferrostatin-1 prevented the increase in SDP ($p < 0.05$ vs. PE group), DBP ($p < 0.05$ vs. PE group), and urinary protein levels ($p < 0.05$ vs. PE group), as well as the reduction in fetal survival rate ($p < 0.05$ vs. PE group). Moreover, the reduction in GSH concentration ($p < 0.05$ vs. PE group, Fig. 9F) and GPx activity ($p < 0.05$ vs. PE group) and the increase in liable Fe(II) ($p < 0.01$ vs. PE group) and MDA concentrations ($p < 0.05$ vs. PE group) was attenuated upon treatment with miR-30b-5p inhibitor. In comparison, ferrostatin-1 prevented only the reduction in GSH concentration ($p < 0.05$ vs. PE group) and the increase in MDA concentrations ($p < 0.05$ vs. PE group).

4. Discussion

Ferroptosis is a newly recognized mechanism of programmed cell death, characterized by iron-dependent accumulation of lipid peroxides. Although oxidative stress has been implicated in the pathogenesis of PE, there is a lack of sufficient evidence to show that ferroptosis occurs in PE. As GSH, GPx, and MDA are important indices to

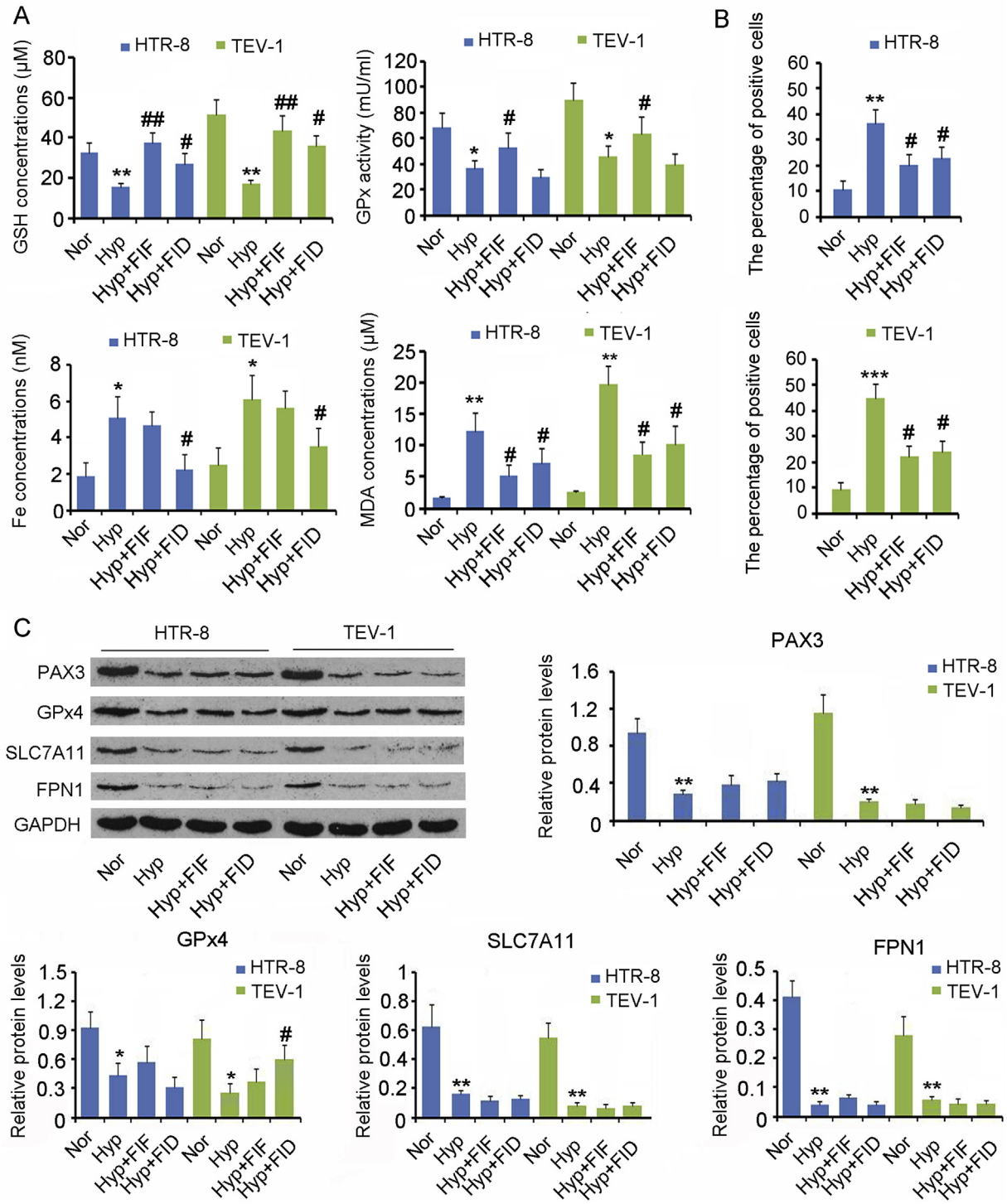

Fig. 5. Effects of ferroptosis inhibitors on ferroptosis of trophoblasts.
The *in vitro* PE model was established by culturing HTR-8/SVneo and TEV-1 cells under hypoxic conditions. Inhibitors of ferroptosis (60 nM Ferrostatin-1 and 100 μM Deferoxamine mesylate) were added to cells cultured under hypoxia. (A) Twenty-4 h later, the GSH content, GPx activity, labile Fe(II) concentration, and MDA content were measured in cells. (B) Intracellular ROS levels were measured using H2DCFDA probe through flow cytometer. (C)Western blot assay was performed to assess the levels of protein closely associated with ferroptosis. FIF: ferroptosis inhibitor, ferrostatin-1; FID: ferroptosis inhibitor deferoxamine mesylate. The mark "*" refers to significance between normoxia and hypoxia groups (*$p < 0.05$, **$p < 0.01$ and ***$p < 0.001$); The mark "#" indicates the significance in comparison of Hyp + FIF and Hyp + FID groups to hypoxia group ($^{\#}p < 0.05$ and $^{\#\#}p < 0.01$). There is no significance between these groups if neither "*" nor "#" was observed above the bar.

evaluate the degree of lipid peroxidation, they can help establish whether ferroptosis occurs in the placenta of patients with PE. In the present study, GSH content and GPx activity were decreased, but the MDA level was increased, in the placenta of patients with PE. Interestingly, D'Souza et al. had reported that the levels of both MDA and GPx were higher in maternal and cord blood in PE [13]. Although the GPx level was higher in the blood, GPx and GSH were still lower in the placenta in PE [13]. GPx4 is the only GPx family member that can

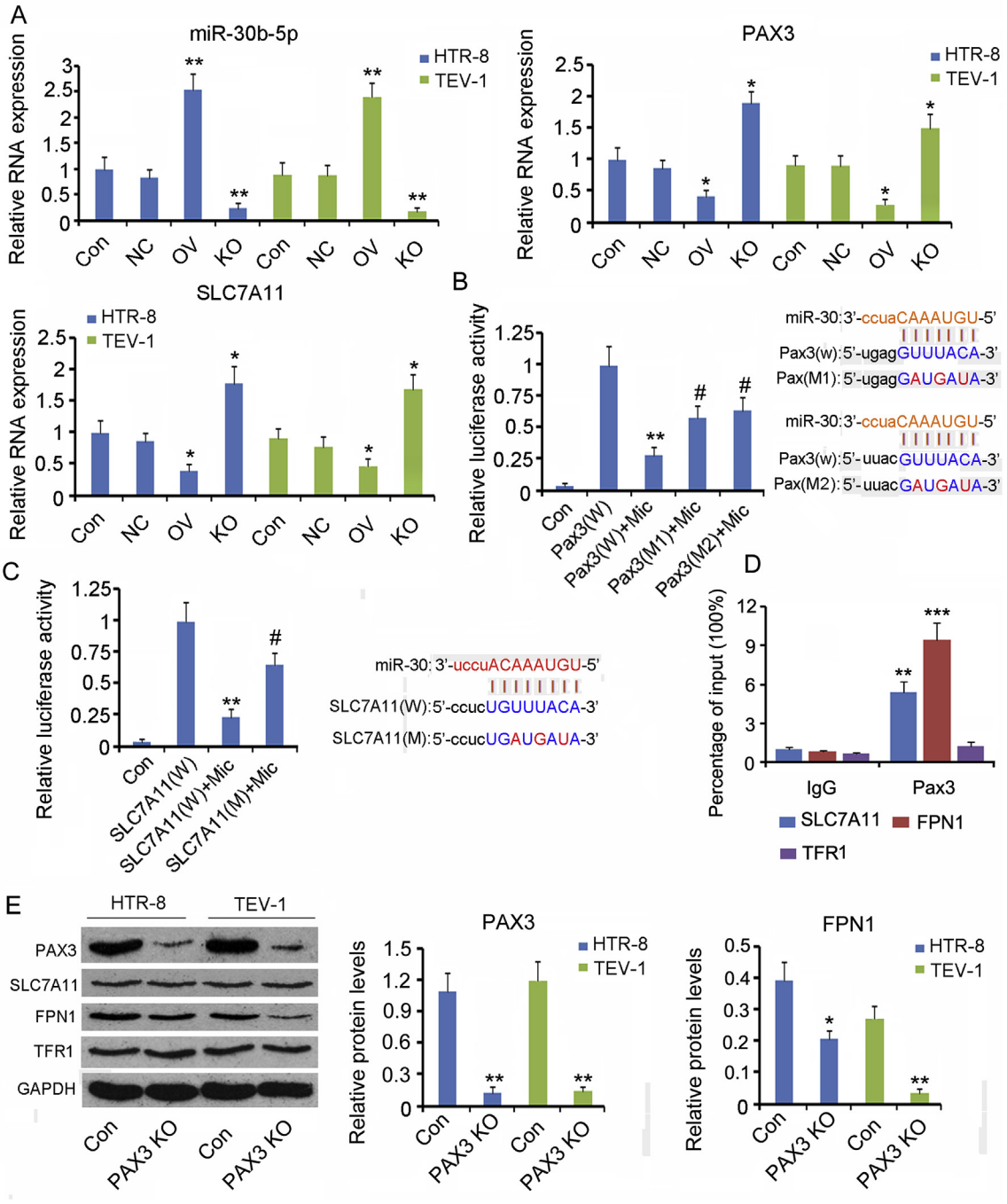

Fig. 6. The regulatory effects of miR-30b-5p and Pax3 on gene expression.

(A) Artificial upregulation and downregulation of miR-30b-5p expression using mimics and inhibitors, respectively. Expression of miR-30b-5p, Pax3, and SLC7A11 in cells was assessed using PCR. NC: transfection of negative control of miRNA vectors; OV: miR-30b-5p overexpression; KO: miR-30b-5p knockdown. $^{*}p < 0.05$, $^{**}p < 0.01$, compared with the control group. (B and C) Luciferase reporter assay was performed to identify the putative binding sites (seed sequences) for hsa-miR-30b-5p in the 3′-UTR of *pax3* and *SLC7A1*1 mRNA, as predicted by the bioinformatic analysis webs, including TargetScan, miRanda, and PicTar. The wild-type (WT) pax3 and SLC7A11 3′-UTR, as well as their mutant versions (MT), with mutations in the putative binding sites, were synthesized and inserted into a pmirGLO vector at XhoI and NotI restriction sites. HTR-8/SVneo cells were transfected with the WT or MT constructs, along with either hsa-miR-10b-3p mimics or negative control. The activity of firefly luciferase was measured and normalized to that of *Renilla* luciferase. Pax3(W): wild-type pax3 constructs; Pax3(M1) and Pax3(M2): two mutant type of Pax3 constructs; SLC7A11(W) and SLC7A11 (M): wild-type and mutant type of Pax3 constructs, respectively; Mimics: hsa-miR-10b-3p mimics. $^{*}p < 0.05$, $^{**}p < 0.01$, compared with the Pax3(W) and SLC7A11(W) groups; $^{\#}p < 0.05$, $^{\#\#}p < 0.01$, compared with the Pax3(W) + Mimics and SLC7A11(W) + Mimics groups. (D) ChIP assay was performed to determine whether Pax3 could bind to the promoters of *SLC7A11*, *FPN1* and *TFR1* genes. $^{**}p < 0.01$, $^{***}p < 0.001$, compared with the IgG group. (E) Pax3 in HTR-8/SVneo and TEV-1 cells was knocked down, followed by the evaluation of protein levels of SLC7A11, FPN1, and TFR1 using western blot assay. Pax3 KO: Pax3 knockdown. $^{*}p < 0.05$, $^{**}p < 0.01$, compared with the control group.

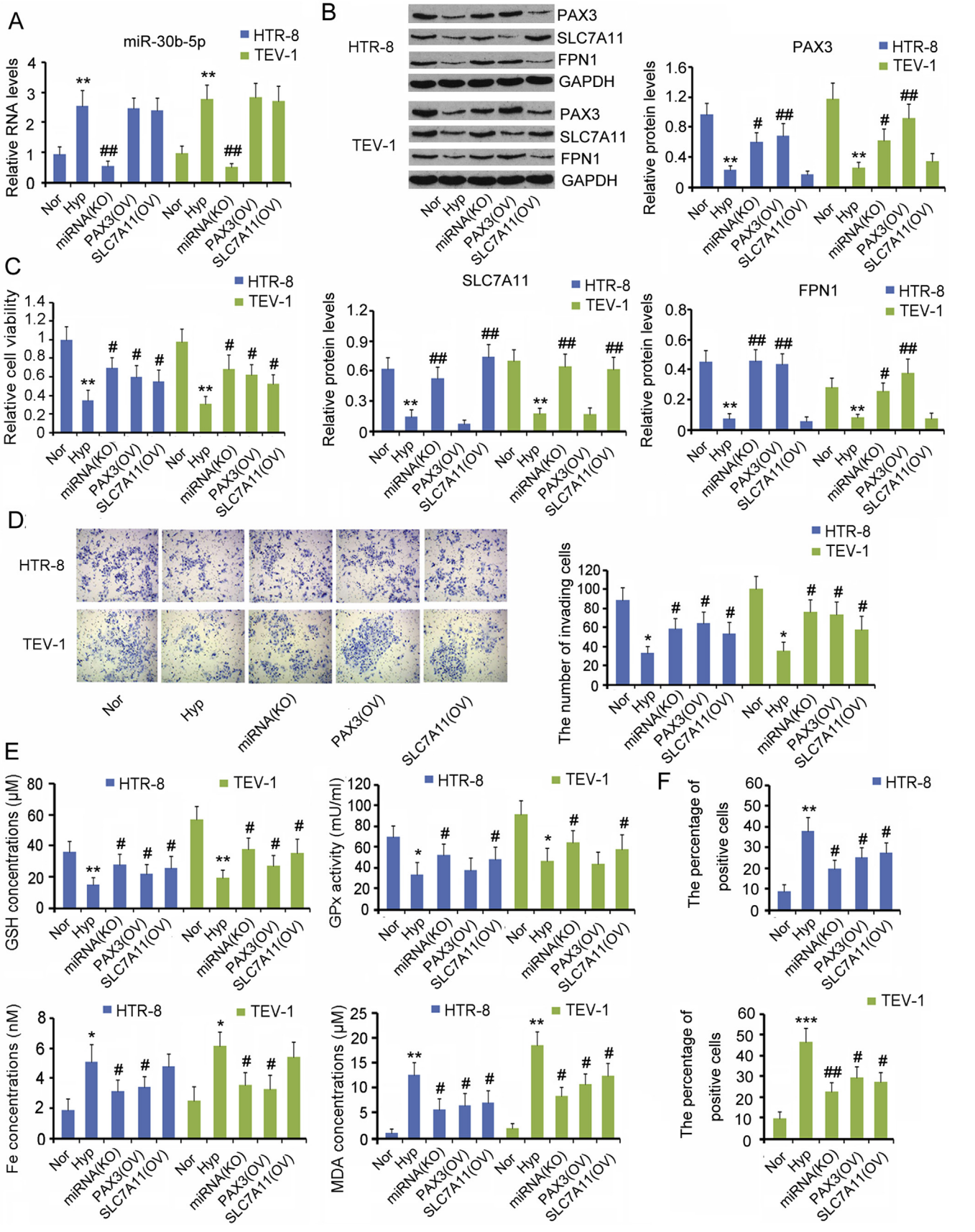

(caption on next page)

Fig. 7. The effects of miR-30b-5p, Pax3, and SLC7A11 on the viability, invasion, and ferroptosis of HTR-8/SVneo and TEV-1 cells.
The *in vitro* PE model was established by culturing HTR-8/SVneo and TEV-1 cells under hypoxic conditions. miR-30b-5p inhibitors, as well as Pax3 and SLC7A11 expression vectors were transfected into cells before the exposure to hypoxia. (A and B) RNA and protein levels of genes were assessed by PCR and western blot assays, respectively. (C and D) Cell viability and invasion capacity were evaluated by CCK-8 agent and transwell method, respectively. (E) GSH content, GPx activity, labile Fe(II) concentration, and MDA content were measured in cells. (F) Intracellular ROS levels were measured using H2DCFDA probe through flow cytometer. $^{*}p < 0.05$, $^{**}p < 0.01$, compared with the HTR-8/SVneo cells under normoxia; $^{\#}p < 0.05$, $^{\#\#}p < 0.01$, compared with the HTR-8/SVneo cells under hypoxia.

block ROS-mediated lipid peroxidation, therefore, GPX4 expression has been used as an important marker for ferroptosis. As indicated by the western blot and IHC assays, the placental levels of GPx4 and SLC7A11 proteins were lower in PE patients than in the control group. In line with our data, Mistry et al. found that the overall immunohistochemical staining of all three GPxs (GPx1, GPx3, and GPx4) in the preeclamptic placenta was lower than that in normotensive placenta, with the most significant reduction observed in GPx4 [14]. Roland-Zejly et al. also found a reduction in GPx4 expression during PE using quantitative PCR, in situ hybridization, and immunohistochemistry assays, independent of the type of delivery (vaginal vs. cesarean) [15]. The expression of SLC7A11 in preeclamptic placenta had never been investigated before, even though it is pivotal for providing cystine for the synthesis of GSH. The reduction in both GPx4 and SLC7A11 suggested a decrease in the efficiency for blocking lipid peroxidation.

Liable Fe(II) is vital for ferroptosis, as it contributes greatly to the generation of lipid peroxides. Numerous studies has confirmed that the total serum iron content is higher in patients with PE than in healthy pregnancy, with Orlov et al. even reporting that the serum iron level has a direct correlation with the blood pressure level [16–18]. However, no study had investigated the level of Fe(II) in placental tissues. Currently, the most fluorescent probes for detecting liable Fe(II) can be used only in live cells. Therefore, we could just measure the total Fe(II) in placental tissues in this study. The total Fe(II) level was higher in the preeclamptic placenta than in normotensive placenta. Intracellular Fe concentration was controlled by import and export transporters. Our results showed that FPN1, which is responsible for the exportation of endogenous iron, was downregulated in the placenta during PE, whereas the expression of FTH1, TFR1, and TFR2, which regulate the import and storage of iron, was not changed. These data suggested that

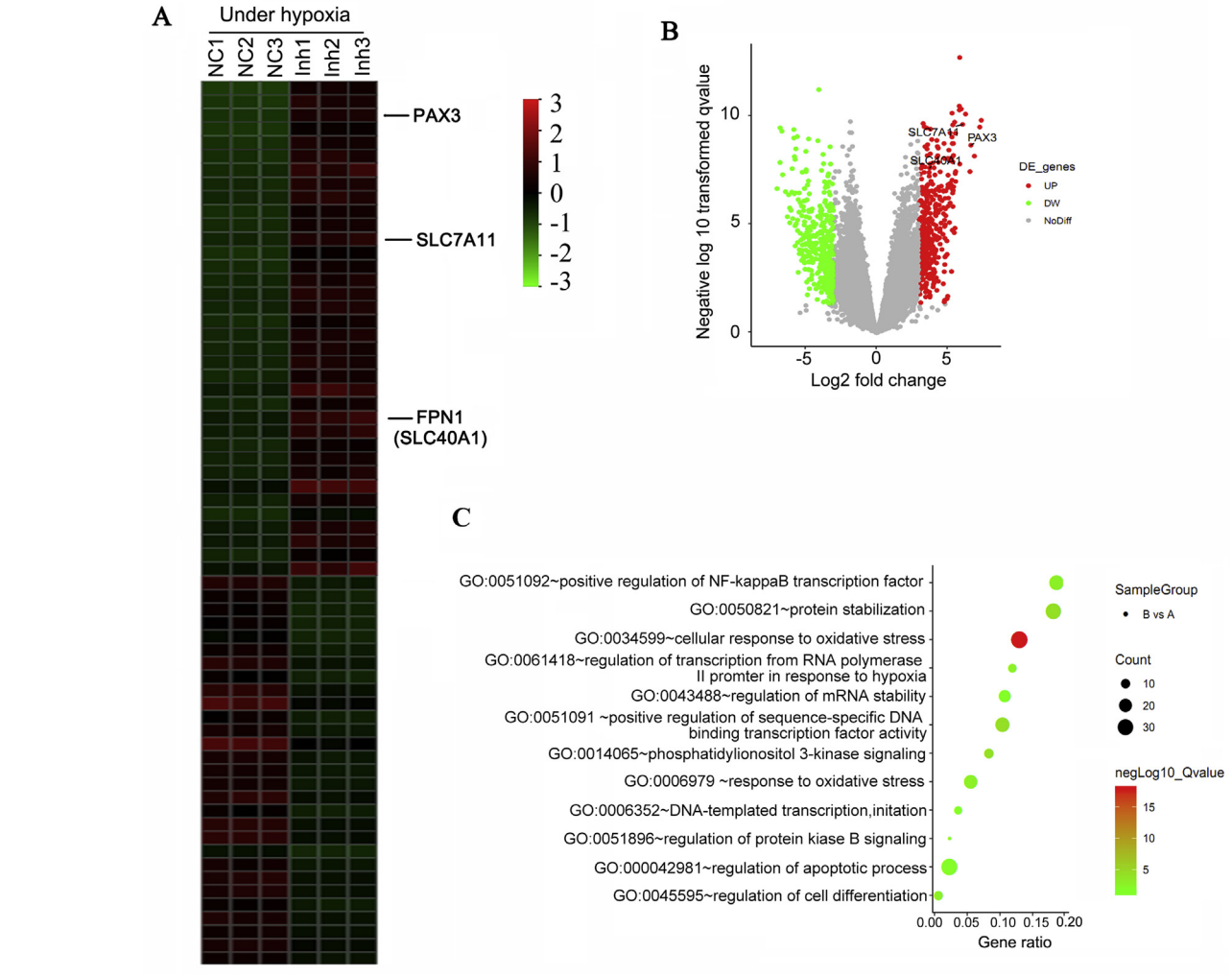

Fig. 8. Biological processes influenced by miR-30b-5p under hypoxia.
Microarray analyses were performed in HTR-8/SVneo cells after down-regulating miR-30b-5p under hypoxia. (A) Heat map shows the differentially expressed genes between miR-30b-5p knockdown and the control groups. NC: negative control; Inh: transfection of miR-30b-5p inhibitor. There were three 3 parallel samples in both NC and Inh groups. (B) Volcanic map shows expression of genes that was significantly up-regulated or down-regulated by miR-30b-5p knockdown. (C) GSEA showed the biological processes affected by miR-30b-5p knockdown.

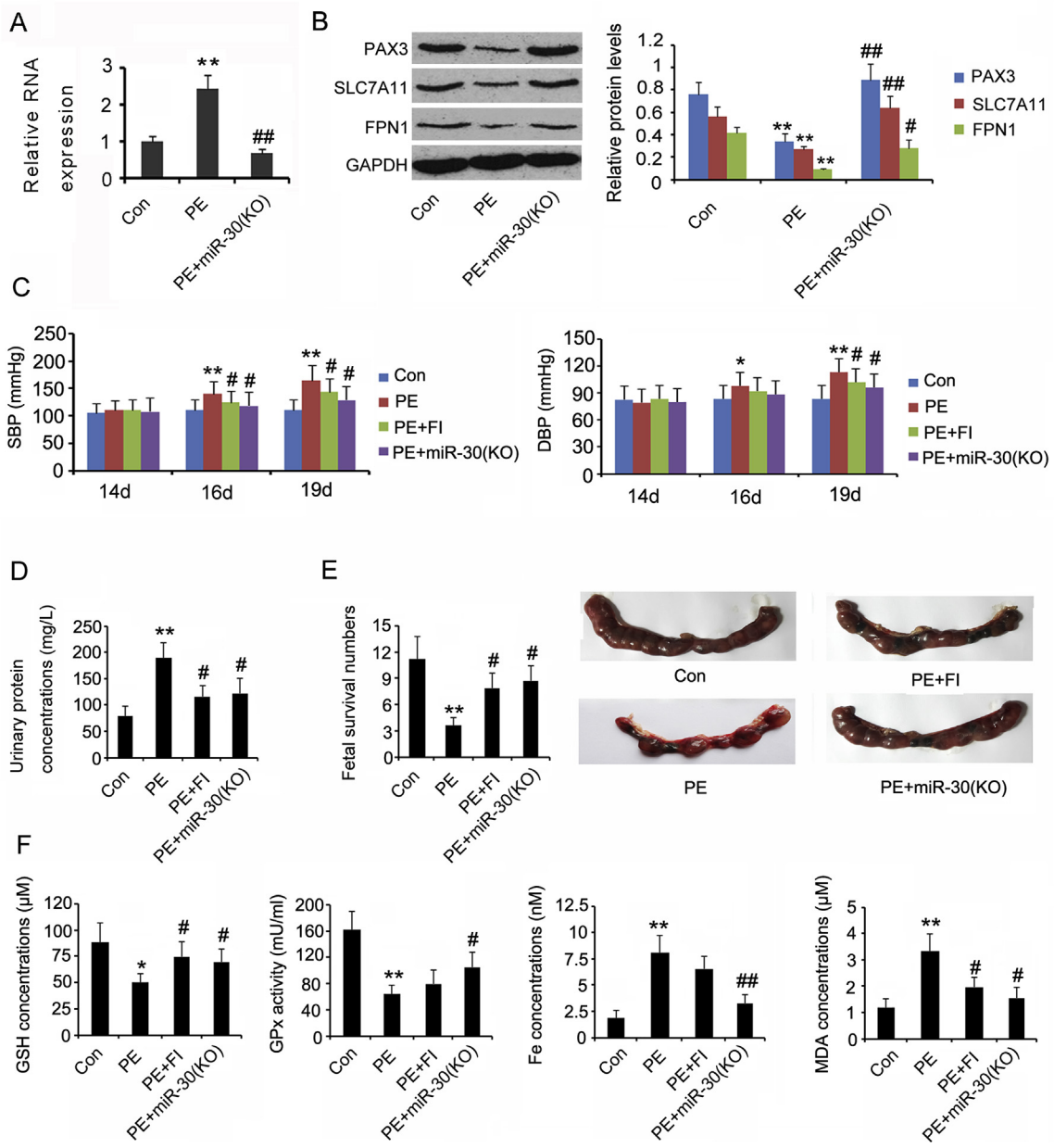

Fig. 9. The therapeutic effects of inhibitors of miR-30b-5p and ferroptosis in PE rat model.
Pregnant SD rats were randomly dived into four groups: sham group (n = 8), PE group (n = 8), PE + ferrostatin-1 group (n = 8) and PE + miR-30b-5p inhibition group (n = 8). On day 14 of pregnancy, PE was induced in the rat model through reduced uterine perfusion pressure (RUPP) surgery. The mini-pump delivered the ferroptosis inhibitor, ferrostatin-1 on day 14 of gestation, at a dose of 10 μmol/kg/day for 5 days. An miR-30b-5p antagonist was injected from the tail veins on day 13 of gestation, at a rate of 100 μL/day for 6 days. (A and B) RNA and protein levels of genes in placental tissues were assessed by PCR and western blot assays, respectively. (C) The blood pressure was measured on days 14, 16, and 19 of gestation, using catheters inserted into the carotid artery and jugular vein. (D and E) Urine protein concentrations and fetal survival rate of the rats were evaluated on day 19 of gestation. (F) GSH content, GPx activity, total Fe(II) concentration, and MDA content were measured in the placental tissues of rats. Con: control rat in sham group; PE: PE rat; miR-30b(KO): inhibition of miR-30b-5p expression by miR-30b-5p antagonist; SDP: systolic blood pressure; DBP: diastolic blood pressure; FI: ferroptosis inhibitor, ferrostatin-1. $^{*}p < 0.05$, $^{**}p < 0.01$, compared with the control. $^{\#}p < 0.05$, $^{\#\#}p < 0.01$, compared with the PE group.

the accumulation of Fe(II) in PE placental tissues is associated with the downregulation of FPN1.

All the abovementioned data suggested that iron-dependent accumulation of lipid peroxides is increased in the PE placenta. Lipid peroxidation plays a pivotal role in endothelial cell dysfunction and death. Gupta et al. previously highlighted the biological association between lipid peroxidation and preeclampsia [19]. MDA is commonly measured as the product of free radical injury on membrane lipids. Plasma level of MDA is significantly higher in preeclamptic pregnancies and is positively correlated with DBP during the early phases of PE [20,21]. Moreover, Tayal et al. found that serum MDA levels are positively correlated with urinary protein and uric acid levels, but negatively correlated with fetal weight in PE patients from India [22]. A longitudinal study showed that the risk of developing PE was 24-fold higher when the MDA levels in maternal erythrocytes were above the cutoff value of 35.98 nmol/g [23]. This cutoff value had a high sensitivity, specificity, and negative predictive value [23]. In addition to MDA in serum and maternal erythrocytes, this study found that the placental MDA levels also had a positive correlation with DBP in patients with PE. GPx, GSH, and Fe(II) are important regulators of lipid peroxidation, and

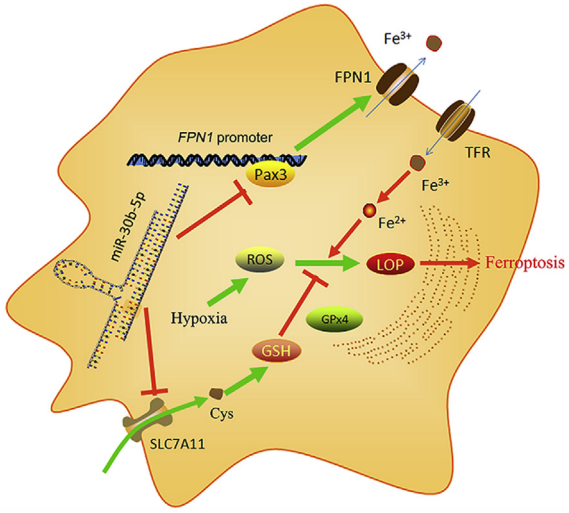

Fig. 10. The mechanism behind ferroptosis induction in trophoblasts by miR-30b-5p under hypoxia.
miR-30b-5p, which targets the 3′-UTR of *Pax3* and *SLC7A11* mRNA, inhibits their expression post-transcriptionally. Downregulation of Pax3 is accompanied with low pre-transcriptional efficiency during FPN1 expression. SLC7A11 and FPN1 regulate the import of cystine and the export of iron, respectively, and therefore, a decreased expression of SLC7A11 and FPN1 blocks the synthesis of GSH and results in the accumulation of iron. With the depletion of GSH, the oxidizing power of ROS that was stimulated by hypoxia was further enhanced by liable Fe(II), leading to a massive generation of lipid peroxides and consequent ferroptosis. GSH: glutathione; FPN1: ferroportin 1; LOP: lipid peroxides; TfR: transferrin receptor.

they also showed A significant correlation with DBP. These data suggested that lipid peroxidation is a leading cause of the damage of maternal systemic circulation in PE.

Although lipid peroxidation occurred in PE placenta, it is uncertain whether trophoblasts and other types of cells in placenta undergo ferroptosis under oxidative stress. Oxidative stress in PE is closely associated with ischemia [24]. Therefore, we established a hypoxia model of trophoblasts *in vitro*, followed by determination of the mode of cell death. As indicated by the diverse detection methods used in this study, trophoblasts underwent apoptosis, autophagy, or necrosis under hypoxic conditions. As there is currently no direct method for the detection of ferroptosis, most studies tend to add ferroptosis inhibitors such as ferrostatin-1 and DFOM, and then measure the change in cell viability, to investigate ferroptosis indirectly. Ferrostatin-1 and DFOM function as a lipid ROS scavenger and an iron-chelating agent, respectively, thereby blocking ferroptosis. Ferrostatin-1 and DFOM have been found to improve the viability of retinal pigment epithelial and neural cells during ROS stress, and therefore, ferroptosis has been suggested to be associated with the pathogenesis of age-related macular and neural degeneration diseases [25,26]. In the present study, both ferrostatin-1 and DFOM treatments increased the trophoblast viability, suggesting that ferroptosis occurred under hypoxic conditions. Although Ferrostatin-1 and DFOM restored GSH levels, GPx activity and Fe/MDA concentrations altered by hypoxia, they had little or no effect on expression of GPx4 (excepted for DFOM increasing GPx4 only in TEV-1 cells), SLC7A11 and FPN1. These data suggested that their inhibitory effect on ferroptosis is almost independent of changing GPx4, SLC7A11 and FPN1 expression. As a lipid ROS scavenger, ferrostatin-1 increasing GSH levels is probably due to the reduction of GSH consumption by ROS. Since DFOM decreased free Fe ions, the oxidative effect of ROS was attenuated, and intracellular GSH levels were conversely increased.

The ferroptosis of trophoblasts under hypoxic conditions is likely associated with the aberrant expression of SLC7A11 and FPN1, which likely resulted in the lack of GSH and intracellular accumulation of free Fe(II). In addition to mRNAs, a large number of miRNAs are also abnormally expressed in the PE placenta, according to the results of the present and previous studies [8–10,27]. miRNAs play an important role in regulating the gene expression at post-transcription levels. Transcription factors, on the other hand, regulate the pre-transcriptional processing of gene expression. The present study revealed that Pax3, a transcription factor belonging to the paired box (PAX) family, is involved in the pre-transcriptional regulation of FPN1 gene. Pax3 plays key roles in cell migration and differentiation as well as organogenesis during embryonic development [28,29]. Our previous study showed that downregulated Pax3 in the PE placenta has been associated with deficient function of trophoblasts [30,31]. The present study suggested that the downregulation of Pax3 is responsible for decreased expression of FPN1 in trophoblasts under hypoxic conditions, as overexpression of Pax3 was able to restore the FPN1 expression. Furthermore, we found that aberrantly upregulated miR-30b-5p in trophoblasts under hypoxic conditions is responsible for the downregulation of both SLC7A11 and Pax3. The inhibition of miR-30b-5p expression, in turn, upregulated SLC7A11, Pax3, and Pax3-downstream target, FPN1, in the trophoblasts. These data suggested that the upregulation of miR-30b-5p is most likely the leading cause of the downregulation of SLC7A11 and FPN1, and the consequent occurrence of ferroptosis in trophoblasts, under hypoxic conditions.

Numerous studies have reported that miR-30b-5p exerts inhibitory effects on cancer proliferation and invasion [32,33]. However, the inhibitory effects of miR-30b-5p on cell proliferation and invasion are expected to be harmful for placental development. The present study showed that inhibiting the upregulation of miR-30b-5p increased the viability and invasive capacity of trophoblasts under hypoxia and attenuated a series of PE symptoms in the rat model. The inhibitory effects of miR-30b-5p on the proliferation and invasion of trophoblasts are likely associated with its promoting effect on ferroptosis, as 1) knockdown of miR-30b-5p and overexpression of SLC7A11 and Pax3 increased the GSE concentration and GPx activity, while decreasing the liable Fe(II) and MDA concentrations, and 2) overexpression of SLC7A11 and Pax3, both of which are downstream to miR-30b-5p and closely associated with the pathogenesis of ferroptosis, also increases cell viability and invasion. A previous study found that an inhibitor of the tumor-driver bromodomain protein BRD4, namely (+)-JQ1, is able to induce the ferroptosis of breast and lung cancer cells [34]. Co-treatment with (+)-JQ1 and ferrostatin-1 (an inhibitor of ferroptosis) restored the viability and invasion ability of cancer cells, both of which were attenuated by (+)-JQ1. However, the viability and invasion ability of cancer cells were reduced more appreciably upon treatment with (+)-JQ1 and 1S,3R-RSL3 (an inducer of ferroptosis) than with either agent alone [34]. These data suggest that cell viability and invasion ability are indeed affected by ferroptosis.

Based on the above mentioned results, we suggest a potential molecular mechanism underlying ferroptosis occurrence in PE placenta (as shown in Fig. 10): abnormally up-regulated miR-30b-5p down-regulated SLC7A11 and Pax3 expression; Pax3 deficiency further caused a low transcript efficiency of FPN1, resulting in its down-regulation; Since SLC7A11 plays a key role in the input of cystine, a substrate for GSH synthesis, SLC7A11 reduction was associated to decreased level of intracellular GSH; FPN1 takes in charge of the export of iron ions, therefore FPN1 reduction led to the accumulation of free iron levels in cells; reduced GSH together with iron accumulation resulted in ferroptosis, which impaired the biological functions of trophoblasts.

Ferroptosis has been proposed as a target for the protection of several types of cells from liver, brain, kidney, intestine, and heart against ischemia or ischemia-reperfusion (I/R) injuries [4,35,36]. Ischemia is a major cause of acute kidney injury (AKI). Through conditional depletion of proteins closely associated with apoptosis and necroptosis, previous studies demonstrated that apoptosis and necroptosis account for only minor damage during AKI [35,36]. However, ferroptosis mediates the regulated and synchronized death of functional

kidney units during ischemia [37,38]. A class of ferroptosis inhibitors, namely ferrostatins, effectively protects against renal ischemia and ischemia-reperfusion (I/R) injuries [38,39]. In addition, intestinal cells usually suffer from ischemia or I/R conditions during small intestinal volvulus, acute mesenteric ischemia, shock, and trauma [4]. Li et al. found that some negative regulators of ferroptosis, such as FTH1 and GPx4, were reduced under ischemia, which sensitized the intestine to ferroptosis during the subsequent oxygen replenishment by reperfusion [40]. However, inhibition of ferroptosis by Liproxstatin-1, a potent and specific ferroptosis inhibitor, attenuated the I/R-induced injury [40]. In the present study, the inhibition of ferroptosis by the inhibitor also attenuated a series of PE symptoms in the rat model. This suggested that ferroptosis indeed plays important role in PE pathogenesis.

The present study for the first time identified that ferroptosis is involved in the pathogenesis of PE. Abnormally up-regulated miR-30b-5p triggered the ferroptosis in trophoblasts under hypoxic conditions by down-regulating SLC7A11, Pax3, and Pax3-downstream target, FPN1. The detail regulatory effects of miR-30b-5p were described in Fig. 10. Blockage of miR-30b-5p up-regulation or direct inhibition of ferroptosis attenuated PE symptoms in the rat model, making miR-30b-5p a potential therapeutic target for PE.

Declaration of competing interest

The authors declare that they have no known competing financial interests or personal relationships that could have appeared to influence the work reported in this paper.

Acknowledgement

This study was supported by Wuxi Kejiao Qiang Wei Key Medical Talent Project (No.ZDRC010), Support Project of Women's Health Care Department of Key Subjects of Maternal And Child Health Care in Jiangsu (No.FXK201703), Maternal and Child Health Research Project in Jiangsu province (No.F201827) and Jiangsu Provincial Science and Technology Department of the Key Disease Standardized Diagnosis and Treatment Project (No. BE2015618).

References

[1] A.A.F. El-Sayed, Preeclampsia: a review of the pathogenesis and possible management strategies based on its pathophysiological derangements, Taiwan. J. Obstet. Gynecol. 56 (5) (2017) 593–598.
[2] M.H. Schoots, S.J. Gordijn, S.A. Scherjon, H. van Goor, J.L. Hillebrands, Oxidative stress in placental pathology, Placenta 69 (2018) 153–161.
[3] K. Matsubara, T. Higaki, Y. Matsubara, A. Nawa, Nitric oxide and reactive oxygen species in the pathogenesis of preeclampsia, Int. J. Mol. Sci. 16 (3) (2015) 4600–4614.
[4] Y. Li, D. Feng, Z. Wang, Y. Zhao, R. Sun, D. Tian, D. Liu, F. Zhang, S. Ning, J. Yao, X. Tian, Ischemia-induced ACSL4 activation contributes to ferroptosis-mediated tissue injury in intestinal ischemia/reperfusion, Cell Death Differ. (2019).
[5] H. Imai, M. Matsuoka, T. Kumagai, T. Sakamoto, T. Koumura, Lipid peroxidation-dependent cell death regulated by GPx4 and ferroptosis, Curr. Top. Microbiol. Immunol. 403 (2017) 143–170.
[6] Y. Zhang, L. Zhuang, B. Gan, BAP1 suppresses tumor development by inducing ferroptosis upon SLC7A11 repression, Mol. Cell Oncol. 6 (1) (2018) 1536845.
[7] D. Chen, Z. Fan, M. Rauh, M. Buchfelder, I.Y. Eyupoglu, N. Savaskan, ATF4 promotes angiogenesis and neuronal cell death and confers ferroptosis in a xCT-dependent manner, Oncogene 36 (40) (2017) 5593–5608.
[8] Z.R. Niu, T. Han, X.L. Sun, L.X. Luan, W.L. Gou, X.M. Zhu, MicroRNA-30a-3p is overexpressed in the placentas of patients with preeclampsia and affects trophoblast invasion and apoptosis by its effects on IGF-1, Am. J. Obstet. Gynecol. 218 (2) (2018) 249.e1–249.e12.
[9] D.S. Jairajpuri, Z.H. Malalla, N. Mahmood, W.Y. Almawi, Circulating microRNA expression as predictor of preeclampsia and its severity, Gene 627 (2017) 543–548.
[10] N.V. Nizyaeva, G.V. Kulikova, M.N. Nagovitsyna, N.E. Kan, K.N. Prozorovskaya, A.I. Shchegolev, G.T. Sukhikh, Expression of MicroRNA-146a and MicroRNA-155 in placental villi in early- and late-onset preeclampsia, Bull. Exp. Biol. Med. 163 (3) (2017) 394–399.
[11] E. Prus, E. Fibach, The labile iron pool in human erythroid cells, Br. J. Haematol. 142 (2) (2008) 301–307.
[12] M.W. Cunningham Jr., J. Castillo, T. Ibrahim, D.C. Cornelius, N. Campbell, L. Amaral, V.R. Vaka, N. Usry, J.M. Williams, LaMarca B2. AT1-AA (Angiotensin II Type 1 Receptor Agonistic Autoantibody) blockade prevents preeclamptic symptoms in placental ischemic rats, Hypertension 71 (5) (2018) 886–893.
[13] V. D'Souza, A. Rani, V. Patil, H. Pisal, K. Randhir, S. Mehendale, G. Wagh, S. Gupte, S. Joshi, Increased oxidative stress from early pregnancy in women who develop preeclampsia, Clin. Exp. Hypertens. 38 (2) (2016) 225–232.
[14] H.D. Mistry, L.O. Kurlak, P.J. Williams, M.M. Ramsay, M.E. Symonds, F. Broughton Pipkin, Differential expression and distribution of placental glutathione peroxidases 1, 3 and 4 in normal and preeclamptic pregnancy, Placenta 31 (5) (2010) 401–408.
[15] L. Roland-Zejly, V. Moisan, I. St-Pierre, J.F. Bilodeau, Altered placental glutathione peroxidase mRNA expression in preeclampsia according to the presence or absence of labor, Placenta 32 (2) (2011) 161–167.
[16] D. Mannaerts, E. Faes, P. Cos, J.J. Briedé, W. Gyselaers, J. Cornette, Y. Gorbanev, A. Bogaerts, M. Spaanderman, E. Van Craenenbroeck, Y. Jacquemyn, Oxidative stress in healthy pregnancy and preeclampsia is linked to chronic inflammation, iron status and vascular function, PLoS One 13 (9) (2018 Sep 11) e0202919.
[17] J.X. Liu, D. Chen, M.X. Li, Y. Hua, Increased serum iron levels in pregnant women with preeclampsia: a meta-analysis of observational studies, J. Obstet. Gynaecol. 39 (1) (2019) 11–16.
[18] Y.P. Orlov, N.V. Govorova, V.N. Lukach, A.V. Mitrofnov, O.D. Dmitriva, Preeclampsia and iron exchange. are there any common patterns? Anesteziol. Reanimatol. 61 (6) (2016) 442–446.
[19] S. Gupta, N. Aziz, L. Sekhon, R. Agarwal, G. Mansour, J. Li, A. Agarwal, Lipid peroxidation and antioxidant status in preeclampsia: a systematic review, Obstet. Gynecol. Surv. 64 (11) (2009 Nov) 750–759.
[20] S. Aydin, A. Benian, R. Madazli, S. Uludag, H. Uzun, S. Kaya, Plasma malondialdehyde, superoxide dismutase, sE-selectin, fibronectin, endothelin-1 and nitric oxide levels in women with preeclampsia, Eur. J. Obstet. Gynecol. Reprod. Biol. 113 (1) (2004) 21–25.
[21] S.K. Jain, R. Wise, Relationship between elevated lipid peroxides, vitamin E deficiency and hypertension in preeclampsia, Mol. Cell. Biochem. 151 (1995) 33–38.
[22] D. Tayal, B. Goswami, S.K. Patra, R. Tripathi, A. Khaneja, Association of inflammatory cytokines, lipid peroxidation end products and nitric oxide with the clinical severity and fetal outcome in preeclampsia in Indian women, Indian J. Clin. Biochem. 29 (2) (2014) 139–144.
[23] M. Basbug, I. Demir, I.S. Serin, et al., Maternal erythrocyte malondialdehyde level in preeclampsia prediction: a longitudinal study, J. Perinat. Med. 31 (2003) 469–474.
[24] A.E. Covarrubias, E. Lecarpentier, A. Lo, S. Salahuddin, K.J. Gray, S.A. Karumanchi, Z.K. Zsengellér, AP39, a modulator of mitochondrial bioenergetics, reduces antiangiogenic response and oxidative stress in hypoxia-exposed trophoblasts: relevance for preeclampsia pathogenesis, Am. J. Pathol. 189 (1) (2019) 104–114.
[25] K. Totsuka, T. Ueta, T. Uchida, M.F. Roggia, S. Nakagawa, D.G. Vavvas, M. Honjo, M. Aihara, Oxidative stress induces ferroptotic cell death in retinal pigment epithelial cells, Exp. Eye Res. 181 (2019) 316–324.
[26] C. Wu, W. Zhao, J. Yu, S. Li, L. Lin, X. Chen, Induction of ferroptosis and mitochondrial dysfunction by oxidative stress in PC12 cells, Sci. Rep. 8 (1) (2018 Jan 12) 574.
[27] L.M. Yamaleyeva, S.H. Lindsey, Potential for miRNAs as biomarkers and therapeutic targets in preeclampsia, Hypertension 69 (4) (2017) 580–581.
[28] C.J. Bae, B.Y. Park, Y.H. Lee, J.W. Tobias, C.S. Hong, J.P. Saint-Jeannet, Identification of Pax3 and Zic1 targets in the developing neural crest, Dev. Biol. 386 (2) (2014 Feb 15) 473–483.
[29] J. Zhang, L. Zhang, X. Liu, F. Zhou, Expression of Cx43 and Pax3 proteins in the human placental villi and decidua during early pregnancy, Bio Med. Mater. Eng. 24 (6) (2014) 3841–3847.
[30] N. Wang, Y. Feng, J. Xu, J. Zou, M. Chen, Y. He, H. Liu, M. Xue, Y. Gu, miR-362-3p regulates cell proliferation, migration and invasion of trophoblastic cells under hypoxia through targeting Pax3, Biomed. Pharmacother. 99 (2018) 462–468.
[31] Y. Feng, J. Wang, Y. He, H. Zhang, M. Jiang, D. Cao, A. Wang, HOXD8/DIAPH2-AS1 epigenetically regulates PAX3 and impairs HTR-8/SVneo cell function under hypoxia, Biosci. Rep. 39 (1) (2019) BSR20182022.
[32] X. Qin, J. Chen, L. Wu, Z. Liu, MiR-30b-5p acts as a tumor suppressor, repressing cell proliferation and cell cycle in human hepatocellular carcinoma, Biomed. Pharmacother. 89 (2017) 742–750.
[33] W. Liu, H. Li, Y. Wang, X. Zhao, Y. Guo, J. Jin, R. Chi, MiR-30b-5p functions as a tumor suppressor in cell proliferation, metastasis and epithelial-to-mesenchymal transition by targeting G-protein subunit α-13 in renal cell carcinoma, Gene 626 (2017) 275–281.
[34] S. Sui, J. Zhang, S. Xu, Q. Wang, P. Wang, D. Pang, Ferritinophagy is required for the induction of ferroptosis by the bromodomain protein BRD4 inhibitor (+)-JQ1 in cancer cells, Cell Death Dis. 10 (5) (2019) 331.
[35] S. Hofmans, T. Vanden Berghe, L. Devisscher, B. Hassannia, S. Lyssens, J. Joossens, et al., Novel ferroptosis inhibitors with improved potency and ADME properties, J. Med. Chem. 59 (2016) 2041–2053.
[36] Q. Li, X. Han, X. Lan, Y. Gao, J. Wan, F. Durham, et al., Inhibition of neuronal ferroptosis protects hemorrhagic brain, JCI Insight 2 (2017) e90777.
[37] M. Gao, P. Monian, N. Quadri, R. Ramasamy, X. Jiang, Glutaminolysis and transferrin regulate ferroptosis, Mol. Cell 59 (2015) 298–308.
[38] A. Linkermann, R. Skouta, N. Himmerkus, et al., Synchronized renal tubular cell death involves ferroptosis, Proc. Natl. Acad. Sci. U. S. A. 111 (47) (2014) 16836–16841.
[39] L.L. Huang, X.H. Liao, H. Sun, X. Jiang, Q. Liu, L. Zhang, Augmenter of liver regeneration protects the kidney from ischaemia-reperfusion injury in ferroptosis, J. Cell Mol. Med. (2019).
[40] Y. Li, D. Feng, Z. Wang, Y. Zhao, R. Sun, D. Tian, D. Liu, F. Zhang, S. Ning, J. Yao, X. Tian, Ischemia-induced ACSL4 activation contributes to ferroptosis-mediated tissue injury in intestinal ischemia/reperfusion, Cell Death Differ. (2019).